

Zooming in on eV-MeV Scale Sterile Neutrinos in light of Neutrinoless Double Beta Decay

Tapoja Jha^{a,b,c*} Sarif Khan^{d,†} Manimala Mitra^{a,b‡} Ayon Patra^{e,§}

^a*Institute of Physics, Sachivalaya Marg, Bhubaneswar, Odisha 751005, India*

^b*Homi Bhabha National Institute, Training School Complex, Anushakti Nagar, Mumbai 400085, India*

^c*School of Physical Sciences, Indian Association for the Cultivation of Science,*

2A & 2B Raja S.C. Mullick Road, Kolkata-700 032, India

^d*Institut für Theoretische Physik, Georg-August-Universität Göttingen,*

Friedrich-Hund-Platz 1, 37077 Göttingen, Germany

^e*Division of Physics, School of Advanced Sciences, VIT University, Chennai Campus, Chennai 600127, India*

Abstract

The existence of light sterile neutrinos, as predicted in several models, can help to explain a number of observations starting from dark matter to recent anomalies in short baseline experiments. In this paper we consider two models - Left-Right Symmetric Zee model and Extended Seesaw model, that can naturally accommodate the presence of light sterile neutrinos in the eV to MeV mass scale. We perform a detailed study on the neutrinoless double beta decay process which receives major contributions from diagrams involving these light sterile neutrinos. Considering a number of theoretical and experimental constraints, including light neutrino masses and mixings, unitarity of the mixing matrix etc., we compare our predicted values of the half-life of neutrinoless double beta decay with the experimental limits. This can put significant constraints on the neutrino mass, active-sterile neutrino mixing and several other important parameters in these models.

Keywords: Sterile neutrino; Neutrinoless double beta decay; Left-right symmetry; Extended Seesaw.

*tapoja.phy@gmail.com

†sarif.khan@uni-goettingen.de

‡manimala@iopb.res.in

§ayon@okstate.edu

Contents

1	Introduction	2
2	Left-Right Symmetric Zee Model and Analysis	4
2.1	Model	5
2.2	Diagrams and amplitudes of $0\nu\beta\beta$ transition	7
2.3	Results	10
3	Extended Seesaw Model and Analysis	16
3.1	Model	16
3.2	Constraints	17
3.3	$0\nu\beta\beta$ decay: sterile neutrino contributions	18
3.4	Analysis:	19
3.4.1	One Generation	19
3.4.2	Three Generation	22
4	Conclusion	26

1 Introduction

The Standard Model (SM) of particle physics, despite its major successes, is unable to explain the observed light neutrino mass splittings and their mixings, which provides a strong motivation to invoke beyond the Standard Model (BSM) physics. The two observed neutrino mass splittings are $\Delta m_{12}^2 \sim 10^{-5} \text{ eV}^2$, $|\Delta m_{13}^2| \sim 10^{-3} \text{ eV}^2$ while the best-fit values of the neutrino mixing angles are $\theta_{12} \sim 34^\circ$, $\theta_{23} \sim 48^\circ$ and $\theta_{13} \sim 8^\circ$ [1]. Though neutrinos are massless in SM, a number of BSM theories have been proposed that successfully explain neutrino masses and mixings. One of the most appealing frameworks to generate Majorana masses of light neutrinos is via seesaw, where the dimension-5 lepton number violating operator generates the mass term after electroweak symmetry breaking [2–8]. The type-I seesaw serves as the most economical framework, as the model in addition to the SM particles is minimally extended by gauge singlet right-handed neutrinos. Another popular class of mechanism is the radiative mass generation [9–13], where neutrino mass is generated via loop effect. In this work, we have considered a variation of the type-I seesaw model referred as Extended Seesaw model [14, 15] and a left-right symmetric extension of radiative neutrino mass model [16–19].

The type-I seesaw model is the most economical, as the SM particle content is expanded with at least two heavy gauge singlet right-handed neutrinos which participate in light neutrino mass generation via seesaw mechanism. However, the drawback of this simplest model is that the mixing of these right-handed neutrinos with SM neutrinos are tightly constrained by eV light neutrino mass constraint, making the detection prospect of these right-handed neutrinos at experiments challenging. In Extended Seesaw, as the name suggests, more singlet neutrinos with large mixings are introduced with the possibility that some of them remain light and can be detected in experiments. The other popular mechanism for neutrino mass

generation is through loop-induced processes. One of the simplest examples of this process is realized in the Zee model where the introduction of a doublet scalar and a charged singlet scalar can generate neutrino masses at the one-loop level. Though the simplest form of Zee model [20] cannot satisfy neutrino oscillation data [21–23], its left-right symmetric extension however is consistent with experimental observations [18, 24]. Here the Majorana mass of the left-handed and right-handed neutrinos are generated at the one-loop level while the Dirac mass term arises at the tree level from the Yukawa interactions. Finally the light neutrino masses are obtained by a type-1 seesaw mechanism but with the exception that the right-handed neutrinos can be light and hence offer better detection prospects.

Both of the above mentioned models can accommodate light right-handed neutrinos with masses ranging in the eV to MeV scale. An eV scale sterile neutrino is well motivated, as this can explain LSND anomaly [25–27]. Recently this anomaly has also been favoured by the MiniBooNE collaboration [28] but at the same time the data has been disfavoured by the KARMEN [29] and MINOS [30] observations. These issues may be finally tackled by the upcoming DUNE experiment [31, 32]. Further hints regarding the presence of an eV scale sterile neutrino comes from the reactor anti-neutrino anomaly (RAA) [33, 34] and the Gallium anomaly [35, 36]. A keV scale sterile neutrino can be an excellent candidate for warm dark matter. Several disagreements between the cosmological observations and the N-body simulations of structure formations can be solved by introducing a keV scale warm dark matter candidate [37]. The presence of an MeV sterile neutrino, on the other hand, can produce several observable astrophysical signals, such as, its effect on the Cosmic Microwave Background spectrum [38] and by producing X-ray photons which may be observable in satellite based X-ray experiments.

If the right-handed neutrinos are Majorana particles, they can give rise to additional contributions to the neutrinoless double beta decay ($0\nu\beta\beta$) process. The $0\nu\beta\beta$ process is the transition $(A, Z) \rightarrow (A, Z+2) + 2e^-$ with no neutrino being emitted [39–41]. The process is lepton number violating [42, 43]. Depending on the mixing of the right-handed neutrinos with active neutrinos in type-I/Extended Seesaw, or the interaction of these right-handed neutrinos with the right-handed gauge boson in left-right symmetric extension, these right-handed neutrino states may give significant contributions in $0\nu\beta\beta$ process compared to the three SM neutrino contributions, and thus opening up the scope of detection of these Majorana neutrinos via $0\nu\beta\beta$ process. A number of experiments have searched for this process and the non-observation of signal has given bound on the half-life $T_{1/2}^{0\nu}$ of $0\nu\beta\beta$ [44–47]. The limit obtained on $T_{1/2}^{0\nu}$ for ^{76}Ge is $T_{1/2}^{0\nu} > 8.0 \times 10^{25}$ year from GERDA-II [44]; whereas, at 90% C.L. the KamLAND-Zen experiment has set a more stringent lower limit on the half-life of ^{136}Xe isotope as $T_{1/2}^{0\nu} > 1.07 \times 10^{26}$ year [45].

In the present work, we consider Left-Right Symmetric Zee model (LRS Zee) and Extended Seesaw model that naturally accommodate light scale sterile neutrinos with masses \sim eV to MeV. Our main goal is to study the $0\nu\beta\beta$ phenomenology for these two models. The left-right symmetric extension of the Zee model [18, 24] presents a unique scenario where the model can be tested at the collider experiments as well as the neutrino experiments. It may have observable signals at the hadron [18, 24] and lepton colliders [19] and most notably can be accessed at the very early stage run of the upcoming e^+e^- colliders. In addition to satisfying all the neutrino mass and mixing constraints, this model can also give rise to several new $0\nu\beta\beta$ process which can significantly enhance the decay rate. This results in a marked decrease in the half-life of the $0\nu\beta\beta$ decay process in this model. We study the variation of $T_{1/2}^{0\nu}$ with respect to different model parameters and identify three of them which are most significant. These three parameters are the lightest neutrino

mass, the Dirac CP phase and the mixing angle between the left and right gauge bosons. By varying these parameters we identify the regions which can be ruled out from the experimental limits on the half-life of $0\nu\beta\beta$ process. In the case of extended seesaw mechanism, we first give an approximate analysis considering only one generation right-handed neutrino and one generation active neutrino. Subsequently, we present a realistic analysis of the half-life with three generation active neutrinos and six generation right-handed neutrinos. We have considered all the constraints arising both from theory and experiments. For the active neutrinos, we have considered bounds on the mass square differences, three mixing angles in agreement with neutrino oscillation data [1] and the limit on the sum of the masses of active neutrinos which comes from Planck satellite experiment [48]. We have ensured a mass hierarchy among these active and right-handed neutrinos to validate the seesaw approximation for this model, as well as have considered constraints from non-unitarity [49]. We have calculated the $0\nu\beta\beta$ decay contribution considering all the required model parameters which pass all the aforementioned constraints and have checked if the predicted contribution satisfies the corresponding experimental limits [45].

The paper is organised in the following way. In Section 2 we present a detailed study of the $0\nu\beta\beta$ process in the LRS Zee model. This is followed by Section 3, where we give a detailed description of extended seesaw scenario and the analysis of the model with respect to many theoretical and experimental aspects, *e.g.*, neutrino oscillation data, $0\nu\beta\beta$ decay, unitarity and others. Finally, we present our conclusions in Section 4.

2 Left-Right Symmetric Zee Model and Analysis

The Zee model [20] is one of the simplest extensions of the Standard Model (SM) which can explain the origin of neutrino mass. By extending the SM framework with an extra doublet and a charged singlet scalar, neutrino masses can be successfully generated at the one-loop level. This simplest form of the Zee model, though, is found to be incompatible with the neutrino experimental data [21–23, 50] and one needs to extend it further in order to get a viable scenario to explain all the neutrino oscillation constraints. The left-right symmetric extension of the Zee model [18, 24] provides an alternate model framework which can easily explain the neutrino oscillation data as well as provide interesting flavor violating signals and unique collider signatures.

The pair production and decay of the singly charged Higgs boson can produce final states with two charged leptons (with either same or different flavors) and missing transverse energy. This process has been studied in the context of the Large Hadron Collider (LHC) in Ref. [18, 24] and for the International Linear Collider (ILC) and the Compact Linear Collider (CLIC) in Ref. [19]. The charged singlet scalar pair-production cross-section at hadron colliders is quite small and is dominated by the photon mediated process, while it can become significantly larger in the electron-positron collider due to the right-handed neutrino mediated t -channel diagram. Thus the ILC and CLIC experiments may be able to observe such a particle with very low integrated luminosity of only 1-3 fb⁻¹, see [19] for details. Below we present a brief discussion on the model.

2.1 Model

Other than the three SM neutrinos, the neutrino sector in this model also contains light right-handed neutrinos with masses ranging from an eV to around 100 eV. Their masses depend on the coupling of right-handed neutrinos with the charged singlet scalar. The Yukawa Lagrangian in this model is given as [18,19,24]

$$\begin{aligned} \mathcal{L}_Y = & Y_{ij}^q \bar{Q}_{Li} \Phi Q_{Rj} + \tilde{Y}_{ij}^q \bar{Q}_{Li} \tilde{\Phi} Q_{Rj} + Y_{ij}^l \bar{l}_{Li} \Phi l_{Rj} + \tilde{Y}_{ij}^l \bar{l}_{Li} \tilde{\Phi} l_{Rj} \\ & + \lambda_{Lij} l_{Li}^T i \tau_2 l_{Lj} \delta^+ + \lambda_{Rij} l_{Ri}^T i \tau_2 l_{Rj} \delta^+ + H.C. \end{aligned} \quad (1)$$

where Φ and δ are the bidoublet and charged singlet scalars with Y and λ being their respective Yukawa couplings. The Majorana masses of all the neutrinos are generated at the one-loop level and as a result, they remain quite light. In order to understand the neutrino sector, we also need to understand the scalar sector of the model.

Charged scalar spectrum: The minimal Higgs sector in this model consists of a bidoublet, two doublets and a charged singlet field given as

$$H_R(1, 1, 2, 1) = \begin{pmatrix} H_R^+ \\ H_R^0 \end{pmatrix}, \quad H_L(1, 2, 1, 1) = \begin{pmatrix} H_L^+ \\ H_L^0 \end{pmatrix}, \quad \Phi(1, 2, 2, 0) = \begin{pmatrix} \phi_1^0 & \phi_2^+ \\ \phi_1^- & \phi_2^0 \end{pmatrix}, \quad \delta(1, 1, 1, 2) = \delta^+. \quad (2)$$

The $SU(2)_R \times U(1)_{B-L}$ symmetry is broken down to $U(1)_Y$ as the neutral component of the right-handed doublet H_R acquires a non-zero vacuum expectation value (VEV). The bidoublet Φ is required to generate the quark and charged lepton masses and Cabibbo-Kobayashi-Maskawa (CKM) mixing angles. The neutrino masses, similar to the Zee model, are generated at the one-loop level due to the presence of the charged singlet scalar field. The charged Higgs bosons play an important role in the generation of the one-loop neutrino masses as their masses and mixings become important parameters in the expression for the induced neutrino Majorana masses. So before we study the neutrino mass generation mechanism it is important to define the mass basis for the charged Higgs bosons. There are in total five charged Higgs states which mix to give five mass eigenstates through the rotation

$$\begin{pmatrix} \phi_1^{-*} \\ \phi_2^+ \\ H_R^+ \\ H_L^+ \\ \delta^+ \end{pmatrix} = V \begin{pmatrix} H_1^+ \\ H_2^+ \\ H_3^+ \\ G_1^+ \\ G_2^+ \end{pmatrix}, \quad (3)$$

where V is the 5×5 charged Higgs mixing matrix. There are three physical Higgs bosons H_1^+, H_2^+, H_3^+ which will contribute to the neutrino masses and two Goldstone states G_1^+, G_2^+ which are eaten up by the W_R and W boson as their longitudinal degrees of freedom. In this model, the ϕ_1^{-*} and the H_R^+ become the Goldstone bosons while the other three charged states mix to form the physical Higgs bosons. Constraints from flavor violating process further require the mass of the second bidoublet scalar ϕ_2^+ to be heavier than around 15 TeV. Thus the largest off-diagonal contributions to V comes from the mixing of the charged singlet δ^+ with the left-handed charged Higgs boson H_L^+ . These elements will play an important role in the neutrino mass generation as well.

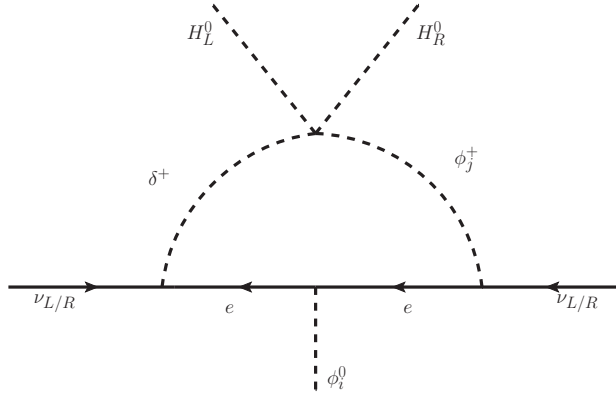


Figure 1: Neutrino Majorana mass generation at one-loop in the LRS Zee model.

Neutrino mass and mixings: The neutrino sector consists of three left-handed and three right-handed neutrinos. The absence of triplet scalars in the model prevents us from writing a Majorana mass term for the neutrinos. All the neutrino Majorana masses here are generated at the one-loop level and hence are quite small. The lightest right-handed neutrino mass ranges from a few eV to a few hundred eV and the other right-handed neutrinos also remain lighter than an MeV. The Dirac masses are thus required to be quite small as well, so as to satisfy the experimentally observed neutrino masses and mixings¹. The one-loop Feynman diagram for the generation of neutrino Majorana masses is given in Fig. 1. The corresponding expressions for the neutrino Majorana masses in this case are given as [24]:

$$\begin{aligned}
 (M_\nu^L)^{\alpha\gamma} &= \frac{1}{4\pi^2} \lambda'_L{}^{\alpha\beta} m_{e_\beta} \sum_{i=1}^3 \text{Log} \left(\frac{M_{h_i}^2}{m_{e_\beta}^2} \right) \times V_{5i} \left[(Y_l^\dagger)^{\beta\gamma} V_{2i}^* - (\tilde{Y}_l^\dagger)^{\beta\gamma} V_{1i}^* \right] + \alpha \leftrightarrow \gamma, \\
 (M_\nu^R)^{\alpha\gamma} &= \frac{1}{4\pi^2} \lambda'_R{}^{\alpha\beta} m_{e_\beta} \sum_{i=1}^3 \text{Log} \left(\frac{M_{h_i}^2}{m_{e_\beta}^2} \right) \times V_{5i} \left[(Y_l)^{\beta\gamma} V_{1i}^* - (\tilde{Y}_l)^{\beta\gamma} V_{2i}^* \right] + \alpha \leftrightarrow \gamma.
 \end{aligned} \tag{4}$$

In the above, $\lambda'_{L/R}{}^{\alpha\beta} = \lambda_{L/R}^{\alpha\beta} - \lambda_{L/R}^{\beta\alpha}$, m_{e_β} and M_{h_i} are the charged lepton and Higgs boson masses and V_{ij} are the charged Higgs boson mixings given in Eq. 3. For our calculations we will consider the case with $\lambda'_L = 0$ as was discussed in [19]. This will thus give us a 6×6 neutrino mass matrix given as

$$M_\nu = \begin{pmatrix} 0 & M_D \\ M_D^T & M_R \end{pmatrix}, \tag{5}$$

where $M_D = Y^l \langle \phi_1^0 \rangle + \tilde{Y}^l \langle \phi_2^0 \rangle$. We thus have a scenario that is very similar to the type-I seesaw mechanism, *i.e.*, the light and heavy neutrino mass matrix after pursuing a block-diagonalization becomes,

$$\mathcal{M}_\nu = -M_D M_R^{-1} M_D^T, \quad \mathcal{M}_n = M_R. \tag{6}$$

The neutrino rotation matrix, taking it from flavor to mass eigenstates, will be a 6×6 matrix which we can write as

$$\mathcal{V} = \begin{pmatrix} \mathbf{U} & \mathbf{S} \\ \mathbf{T} & \mathbf{V} \end{pmatrix}, \tag{7}$$

¹Detailed analysis of the neutrino sector of LRS Zee model is presented in Ref. [19]

such that

$$\mathcal{V}^T M_\nu \mathcal{V} = \begin{pmatrix} \widehat{M}_\nu & 0 \\ 0 & \widehat{M}_N \end{pmatrix}. \quad (8)$$

Here $\widehat{M}_\nu = \text{diag}(m_1, m_2, m_3)$ and $\widehat{M}_N = \text{diag}(M_1, M_2, M_3)$ are diagonal matrices consisting of the light and heavy neutrino masses, respectively.

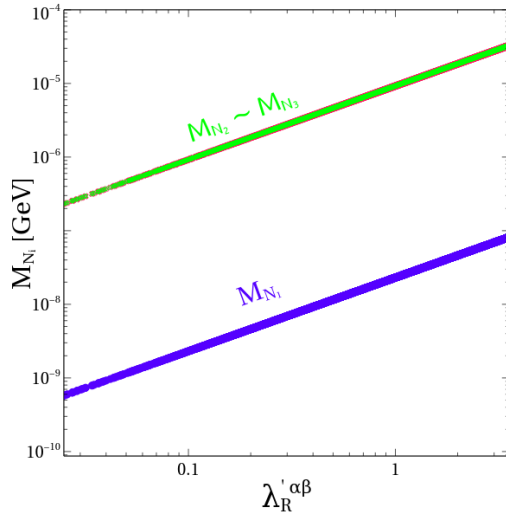


Figure 2: Right-handed neutrino Majorana mass in the LRS Zee model [19].

Fig. 2 shows a plot of the Majorana masses of the right-handed neutrinos as generated at the one-loop level in this model. The plot shows the variation of the eigenvalues of the right-handed neutrino Majorana mass matrix (elements of the matrix given in Eq. 4) as a function of its coupling with the charged singlet scalar. As λ'_R is varied from 0.1 to 3, the lightest right handed neutrino mass M_{N_1} varies from 3 eV to 80 eV, while $M_{N_{2,3}}$ remain in the sub-MeV scale. In generating the plot, we considered the lightest charged Higgs boson has a mass 473 GeV, which primarily consists of charged singlet δ . Below we discuss the contribution of the right-handed neutrinos in $0\nu\beta\beta$ decay.

2.2 Diagrams and amplitudes of $0\nu\beta\beta$ transition

Contrary to most seesaw models which contain the right-handed neutrinos of TeV scale mass, the LRS Zee model naturally accommodates eV-MeV scale right-handed neutrinos, as has already been discussed in the previous section. Diagrams involving the right-handed neutrinos can thus significantly contribute to the $0\nu\beta\beta$ processes and this model gives us an excellent framework to study these effects.

The Feynman diagrams of all the possible contributions are presented in Fig 3. For each diagram we write its amplitude and identify the dimensionless parameter η_i that will be used in the computation of the half life ($T_{1/2}^{0\nu}$) of the $0\nu\beta\beta$ process. In the subsequent discussion, we refer the mass eigenstates of SM neutrinos

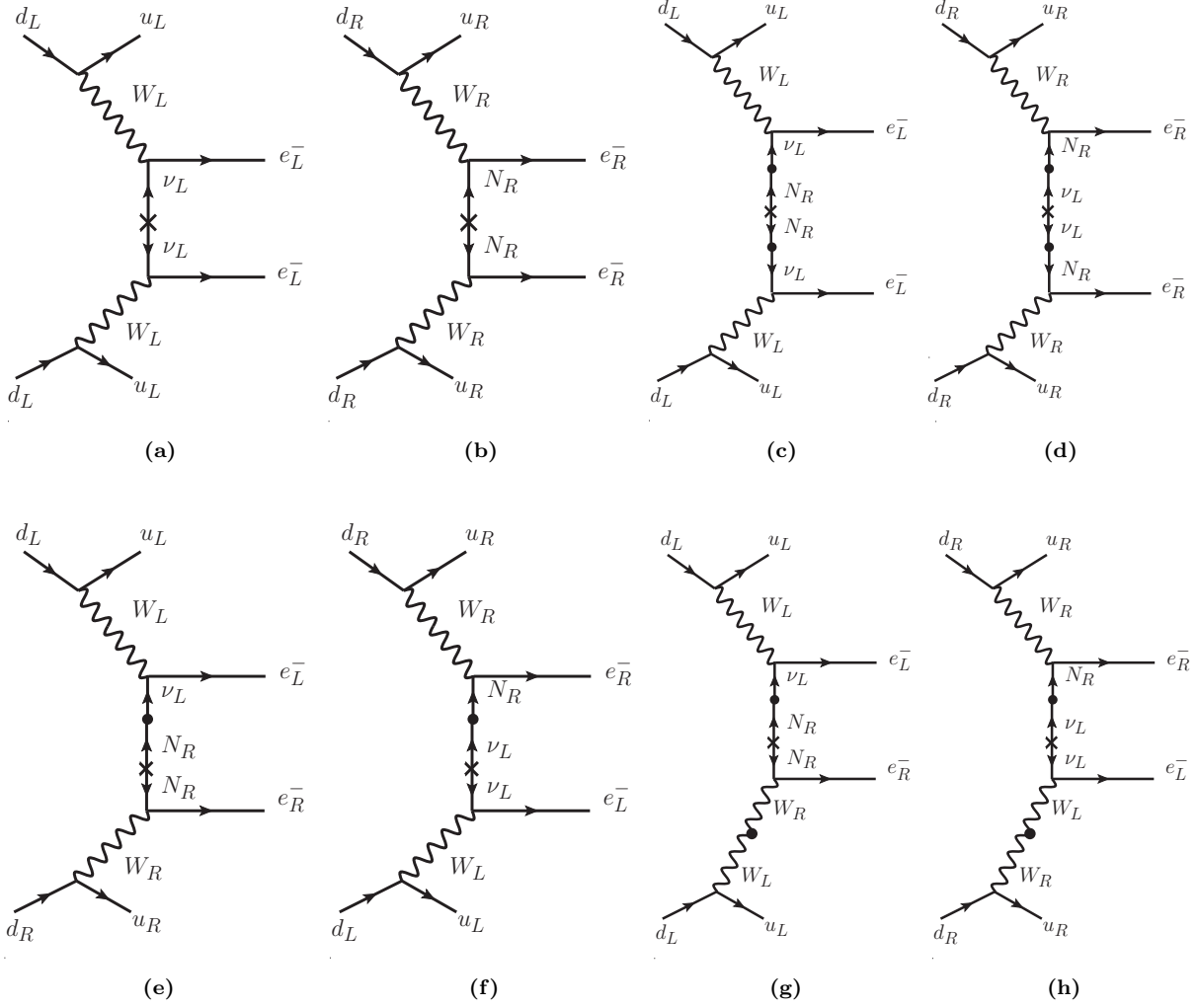


Figure 3: Feynman diagrams of all possible $0\nu\beta\beta$ processes in the LRS Zee model.

as ‘light’, and the right-handed neutrinos as ‘heavy’, as the right-handed neutrino states are heavier than the SM neutrinos.

- *Light neutrino diagram:* The diagram (a) corresponds to the light neutrino contribution. Its amplitude is given as

$$A_1 \simeq G_F^2 \sum_i \mathbb{U}_{ei}^2 \frac{m_i}{p^2}, \quad (9)$$

where G_F is the Fermi constant, p is the momentum transfer at the leptonic vertex and $i = 1, 2, 3$ corresponds to the light neutrino mass eigenstates. The corresponding η obtained in this case is given as

$$\eta_1 = \frac{1}{m_e} \sum_i \mathbb{U}_{ei}^2 m_i. \quad (10)$$

- *Heavy neutrino diagrams:* Diagram (b) corresponds to the heavy neutrino contribution. The heavy neutrinos in this model are composed of the right-handed neutrinos but unlike other Left-Right models, they are quite light in this case with masses in the eV to MeV range. The Feynman amplitude and the corresponding η from this diagram is given as

$$A_2 \simeq G_F^2 \left(\frac{M_{W_L}}{M_{W_R}} \right)^4 \sum_i \mathbb{V}_{ei}^2 \frac{M_i}{p^2}, \quad \eta_2 = \frac{1}{m_e} \left(\frac{M_{W_L}}{M_{W_R}} \right)^4 \sum_i \mathbb{V}_{ei}^2 M_i, \quad (11)$$

where the summation is over the heavy neutrino eigenstates in this case.

- *Light-heavy neutrino mixing diagram:* Diagrams (c) & (d) correspond to the contributions due to the mixing between the light and heavy neutrinos. The Feynman amplitudes are given as

$$A_3 \simeq G_F^2 \sum_i \mathbb{S}_{ei}^2 \frac{M_i}{p^2}, \quad A_4 \simeq G_F^2 \left(\frac{M_{W_L}}{M_{W_R}} \right)^4 \sum_i \mathbb{T}_{ei}^2 \frac{m_i}{p^2}, \quad (12)$$

while the η factors are

$$\eta_3 = \frac{1}{m_e} \sum_i \mathbb{S}_{ei}^2 M_i, \quad \eta_4 = \frac{1}{m_e} \left(\frac{M_{W_L}}{M_{W_R}} \right)^4 \sum_i \mathbb{T}_{ei}^2 m_i. \quad (13)$$

- λ *diagrams:* Diagrams (e) & (f) represent the processes mediated by the $W_L - W_R$ exchange. The Feynman amplitudes from each diagram can be easily combined to give us a final expression which is

$$A_\lambda \simeq G_F^2 \left(\frac{M_{W_L}}{M_{W_R}} \right)^2 \sum_i \frac{\mathbb{U}_{ei} \mathbb{T}_{ei}^* + \mathbb{V}_{ei} \mathbb{S}_{ei}^*}{p}, \quad (14)$$

and the expression for the η parameter is

$$\eta_\lambda = \left(\frac{M_{W_L}}{M_{W_R}} \right)^2 \sum_i \mathbb{U}_{ei} \mathbb{T}_{ei}^* + \mathbb{V}_{ei} \mathbb{S}_{ei}^*. \quad (15)$$

- η *diagrams:* Diagrams (g) & (h) are due to the $W_L - W_R$ mixing in this model and depend on the $W_L - W_R$ mixing angle θ_{LR} . The Feynman amplitude combining the two diagrams can be written as

$$A_\eta = G_F^2 \tan \theta_{LR} \sum_i \frac{\mathbb{U}_{ei} \mathbb{T}_{ei}^* + \mathbb{V}_{ei} \mathbb{S}_{ei}^*}{p} \quad (16)$$

and the corresponding η parameter is

$$\eta_\eta = \tan \theta_{LR} \sum_i \mathbb{U}_{ei} \mathbb{T}_{ei}^* + \mathbb{V}_{ei} \mathbb{S}_{ei}^*. \quad (17)$$

The half-life for the $0\nu\beta\beta$ process after combining the contributions from all these diagrams is then given as [51–54]

$$T_{1/2}^{0\nu} = \left[G_{0\nu} \left(|M_\nu^{0\nu} \eta_1 + M_\nu^{0\nu} \eta_3|^2 + |M_\nu^{0\nu} \eta_2 + M_\nu^{0\nu} \eta_4|^2 + |M_\lambda^{0\nu} \eta_\lambda + M_\eta^{0\nu} \eta_\eta|^2 \right) \right]^{-1}, \quad (18)$$

where $G_{0\nu}$ is the phase space factor; $M_\nu^{0\nu}$, $M_\lambda^{0\nu}$ and $M_\eta^{0\nu}$ are the nuclear matrix elements.

Now that we have the expression for the half-life for the $0\nu\beta\beta$ processes, let us discuss some of the features of this framework which will help us understand the relative contribution arising from each of these diagrams. The right-handed neutrino masses being at the eV to MeV scale contribute significantly to these processes here and hence the diagrams involving N_R become quite important. The relative contributions from the diagrams are also highly dependent on the light-heavy neutrino mixings (\mathbb{S} , \mathbb{T}) with the λ and η diagrams becoming significant as this mixing increases. The gauge boson ($W_L - W_R$) mixing is another important factor in these diagrams and its value can determine which diagram gives significant contribution to the $0\nu\beta\beta$ decay process. Finally since the W_R boson mass is required to be quite large from experimental constraints [55–67], we have chosen it to be 5.5 TeV here and this results in a large suppression for all the diagrams with amplitudes involving $(M_{W_L}/M_{W_R})^4$ term.

The neutrino parameters in this model depend significantly on the masses and mixings of the charged scalars as can be seen quite clearly from Eq. 4. A close inspection of this equation also shows that the factor V_{5i} which is the mixing between the charged singlet and other charged Higgs states is quite important for the neutrino masses. As discussed earlier, the charged singlet Higgs δ^+ can only have significant mixing with the left-handed charged scalar H_L^+ . We can thus approximately write

$$\begin{aligned} H_1^+ &= \delta^+ \cos \theta + H_L^+ \sin \theta, \\ H_2^+ &= -\delta^+ \sin \theta + H_L^+ \cos \theta, \end{aligned} \tag{19}$$

where H_1^+ and H_2^+ are the lightest and next-to-lightest charged Higgs bosons respectively with θ being the mixing angle. Clearly two extreme cases appear here

1. maximal mixing with $\theta = \pi/4$, denoted as H_{\max} ,
2. minimal mixing with $\theta = 0$, denoted as H_{\min} .

2.3 Results

To analyse the half-life of $0\nu\beta\beta$ process for Germanium (^{76}Ge) and Xenon (^{136}Xe) nucleus, we consider two cases of maximal and minimal mixing as described in the previous section. We consider a normal mass ordering among the SM neutrinos, and use the Casas-Ibarra [68] parametrization to fit the latest neutrino oscillation data [1]. As the right-handed neutrino masses are quite small here, the mixing between them and the left-handed neutrinos, represented by the \mathbb{S} and \mathbb{T} matrices in Eq. 7, can become quite significant². For a fixed choice of the right-handed neutrino masses, the light-heavy neutrino ($\nu_L - N_R$) mixing depends largely on the light neutrino masses. As the SM neutrino masses increase, the mass difference between the light and heavy neutrino states become smaller resulting in a larger mixing angle. Thus the lightest neutrino mass m_{ν_1} is an important parameter for our analysis.

The other parameters which play a significant role in determining the value of $T_{1/2}^{0\nu}$ are the $W_L - W_R$ mixing angle (θ_{LR}) and the Dirac CP phase (δ_{CP}) of the neutrino Pontecorvo-Maki-Nakagawa-Sakata (PMNS) matrix. The contribution from the η diagram, directly proportional to $\tan \theta_{LR}$, can become substantial depending on this mixing angle. The value of δ_{CP} , though directly does not appear in any of the expressions,

²These terms still remain orders of magnitude smaller than the \mathbb{U} and \mathbb{V} matrices.

determines the neutrino parameters obtained from the Casas-Ibarra parametrization. This has a significant consequence on the calculated value of $T_{1/2}^{0\nu}$. The nuclear matrix elements (NMEs) for ^{76}Ge and ^{136}Xe , which we adopt from [44, 45] are equally important for the evaluation of $T_{1/2}^{0\nu}$. We consider two cases, one with the maximum and another with the minimum values of the NMEs, and evaluate the half-life. For each nucleus (^{76}Ge or ^{136}Xe), we thus get four separate cases which are:

- (a) $\mathbf{H}_{\min} - (^{76}\text{Ge}/^{136}\text{Xe})_{\min}$: Corresponds to the case where the Higgs boson mixing is minimum and minimum value for the $^{76}\text{Ge}/^{136}\text{Xe}$ NME has been used.
- (b) $\mathbf{H}_{\max} - (^{76}\text{Ge}/^{136}\text{Xe})_{\min}$: Corresponds to the case where the Higgs boson mixing is maximum and minimum value for the $^{76}\text{Ge}/^{136}\text{Xe}$ NME has been used.
- (c) $\mathbf{H}_{\min} - (^{76}\text{Ge}/^{136}\text{Xe})_{\max}$: Corresponds to the case where the Higgs boson mixing is minimum and maximum value for the $^{76}\text{Ge}/^{136}\text{Xe}$ NME has been used.
- (d) $\mathbf{H}_{\max} - (^{76}\text{Ge}/^{136}\text{Xe})_{\max}$: Corresponds to the case where the Higgs boson mixing is maximum and maximum value for the $^{76}\text{Ge}/^{136}\text{Xe}$ NME has been used.

For each of these cases we vary m_{ν_1} , θ_{LR} and δ_{CP} to obtain the predicted value of the half-life of $0\nu\beta\beta$ decay process. Fig. 4 shows the variation of $T_{1/2}^{0\nu}$ for ^{76}Ge nucleus as a function of the lightest neutrino mass

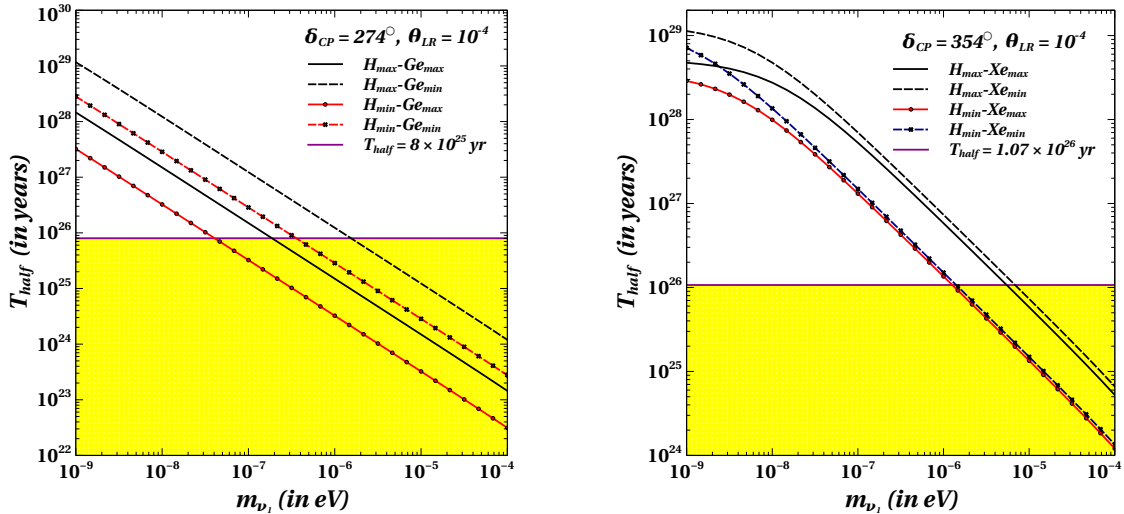


Figure 4: Half-life of $0\nu\beta\beta$ process for ^{76}Ge and ^{136}Xe nucleus as a function of lightest neutrino mass. The shaded region correspond to $T_{1/2}^{0\nu} < 8.0 \times 10^{25}$ years for left panel, and 1.07×10^{26} years for right panel and disallowed by GERDA [44], and KamLAND-Zen [45], respectively.

m_{ν_1} for a fixed value of θ_{LR} and δ_{CP} . The values of all other PMNS matrix elements were fixed to their central values and the λ'_R matrix was chosen such that the right-handed neutrino masses were 7.92 eV, 3.54 keV and 3.55 keV respectively. As can be seen here, the half-life decreases quite drastically as the lightest neutrino mass increases. This is because the light-heavy neutrino mixing increases as discussed earlier and as a result the η_3 , η_λ and η_η contributions become dominant. As for this figure, we consider a large value

of θ_{LR} , therefore η_η always dominate. We find that the canonical light neutrino contribution η_1 is rather subdominant in this figure.

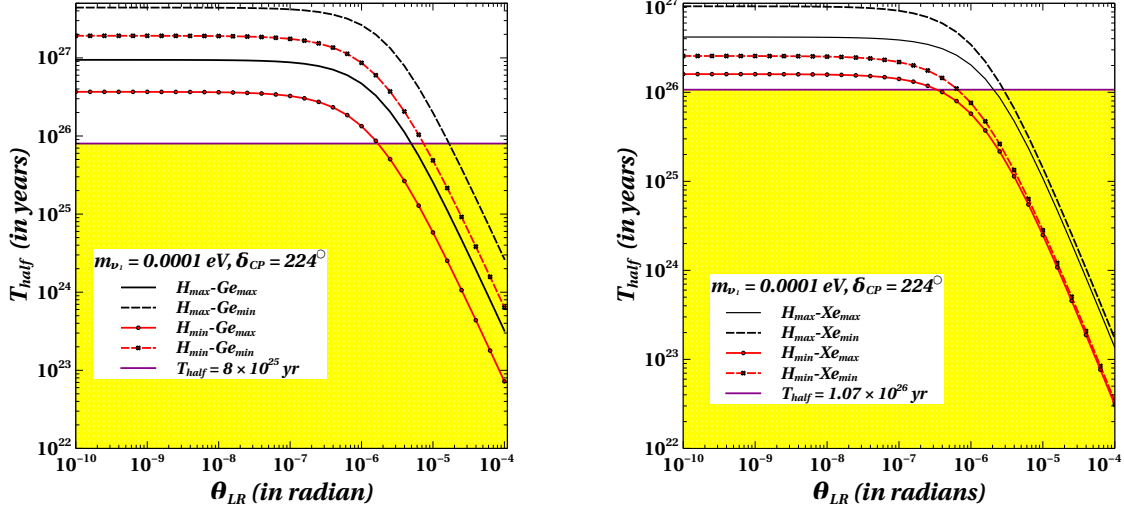


Figure 5: Half-life of $0\nu\beta\beta$ process for ^{76}Ge (left panel) and ^{136}Xe nucleus (right panel) as a function of left-right charged gauge boson mixing.

Fig. 5 shows the variation of $T_{1/2}^{0\nu}$ with the left-right charged gauge boson mixing θ_{LR} . As θ_{LR} increases the decay half-life falls drastically for a value $\theta_{LR} \gtrsim 10^{-6}$. This is the point at which the η_η term, which is proportional to $\tan\theta_{LR}$ starts dominating over the other terms resulting in a steep decrease of the half-life as expected. For smaller value of θ_{LR} , the dominant contribution arises from $\eta_1, \eta_3, \eta_\lambda$, which are independent of the left-right mixing. Since the CP violating phase δ_{CP} is another crucial parameter in our analysis, we show the variation of half-life with respect to δ_{CP} . Fig. 6 gives the change of $T_{1/2}^{0\nu}$ for ^{76}Ge nucleus as a function of δ_{CP} . A close inspection of the numbers we obtained shows that the variation of half-life mirrors the variation in $\sin\delta_{CP}$ which directly determines the values of the neutrino parameters obtained in our calculations. This is to note that, in all these figures, the scenario $H_{\min} - G_{\max}$ gives the strongest constraint. This can be understood from the expression of $T_{1/2}^{0\nu}$ as given in Eq. 18. As can be seen, the calculated half-life is smaller (leading to a more constrained scenario) for larger values of the amplitudes and NMEs. Therefore, naturally the maximum values of ^{76}Ge NMEs leads to a more constrained scenario.

The charged Higgs mixing on the other hand plays an indirect but significant role in determining the values obtained for the Feynman diagram amplitudes. As was discussed earlier, the Feynman amplitudes corresponding to η_2 , and η_4 are negligible due to the $(M_{WL}/M_{WR})^4$ suppression. So the dominant contribution always arises from any one of the η_1, η_λ or η_η terms, while we find η_3 contribution is slightly smaller than these above mentioned contributions. A smaller charged Higgs mixing will invariably lead to a lighter Majorana mass for the RH neutrinos, which has a two-fold effect on the neutrino sector. Firstly, lighter RH neutrinos will result in relatively heavier active neutrinos since the active neutrino mass is obtained by seesaw mechanism in our case. This will boost the η_1 amplitude resulting in a smaller value of $T_{1/2}$. Secondly, a heavier active neutrino will result in a larger light-heavy mixing as discussed earlier. This again

helps boost the η_λ and η_η amplitudes further lowering the calculated half-life of $0\nu\beta\beta$ process, leading to a tight constraint on the parameter.

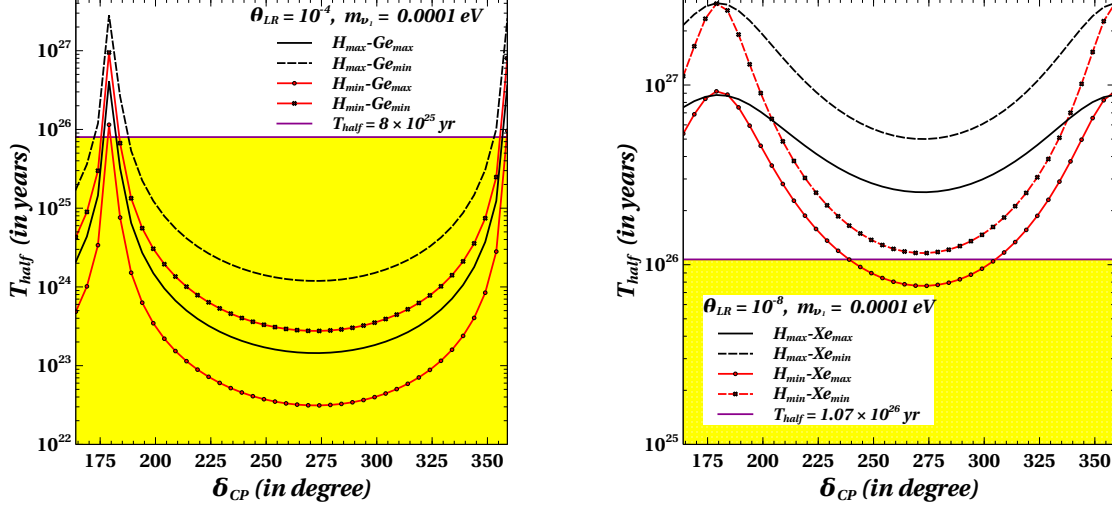


Figure 6: Half-life of $0\nu\beta\beta$ process for ^{76}Ge and ^{136}Xe nucleus as a function of CP violating phase in the PMNS matrix.

The plots obtained for the ^{136}Xe nucleus are very similar in nature to the ones for ^{76}Ge and the most constrained scenario is again the $H_{\min} - \text{Xe}_{\max}$ case. This warrants for a more detailed study of this particular case for a better understanding, which we discuss below. We present the results for both ^{76}Ge and ^{136}Xe nucleus in the ensuing discussion of the most constrained scenario for each, i.e., largest values for the NMEs and minimal mixing of the Higgs sector $H_{\min} - \text{Ge}_{\max}$ and $H_{\min} - \text{Xe}_{\max}$.

Fig. 7 shows the variation of $T_{1/2}^{0\nu}$ for ^{76}Ge as a function of the lightest neutrino mass for several fixed values of θ_{LR} and δ_{CP} . It is quite clear that the value of $T_{1/2}^{0\nu}$ decreases as the lightest neutrino mass and/or value of θ_{LR} increases. The variation with m_{ν_1} is quite evident from our earlier discussion. For the set of plots with $\theta_{LR} = 10^{-8}$, the initial variation with m_{ν_1} is quite modest till $m_{\nu_1} \lesssim 10^{-7}$ eV. The major contribution here comes from the η_1 term with the half-life slowly decreasing with an increase in the lightest neutrino mass. At larger values of m_{ν_1} , the light-heavy neutrino mixing increases significantly and the dominant contribution comes from the η_λ term. The effect of increasing θ_{LR} can be understood as an artefact of an increase in the η_η term which starts contributing quite significantly at $\theta_{LR} \gtrsim 10^{-6}$. Similar characteristics and dependence can be observed in Fig. 8 where we have plotted the variation of $T_{1/2}^{0\nu}$ as a function of θ_{LR} for fixed values of m_{ν_1} and δ_{CP} . As can be seen here, the value of $T_{1/2}^{0\nu}$ remain almost constant in the initial region of $\theta_{LR} \lesssim 10^{-6}$. In this region, the dominant contribution comes from η_1 and η_λ and since the lightest neutrino mass is constant for each line, there is no variation in their value. In the region $\theta_{LR} \gtrsim 10^{-6}$, the η_η term starts dominating and we see a sharp decrease in the value of $T_{1/2}^{0\nu}$ in this region.

Finally, the variation of $T_{1/2}^{0\nu}$ with δ_{CP} is given in Fig. 9. This plot is quite interesting as it clearly shows the contribution of different η terms in different regions of parameter space. The line corresponding to $\theta_{LR} = 10^{-8}$ and $m_{\nu_1} = 10^{-9}$ eV has a dominant contribution from η_1 term. As $\eta_1 = \frac{1}{m_e} \sum_i \mathbb{U}_{ei}^2 m_i$, its contribution in this case only depends on the matrix elements \mathbb{U}_{ei} since m_e and m_i remains constant. The \mathbb{U}_{13}

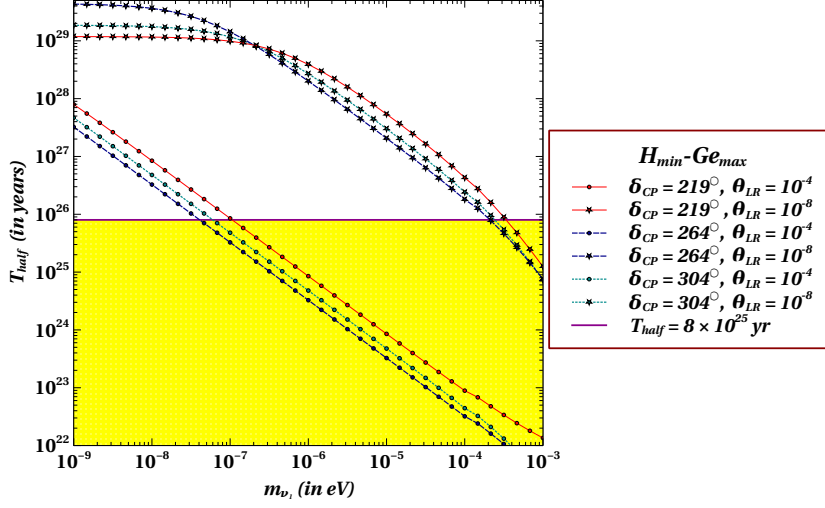


Figure 7: Half-life of $0\nu\beta\beta$ process for ^{76}Ge nucleus as a function of the the lightest neutrino mass for several fixed values of θ_{LR} and δ_{CP} .

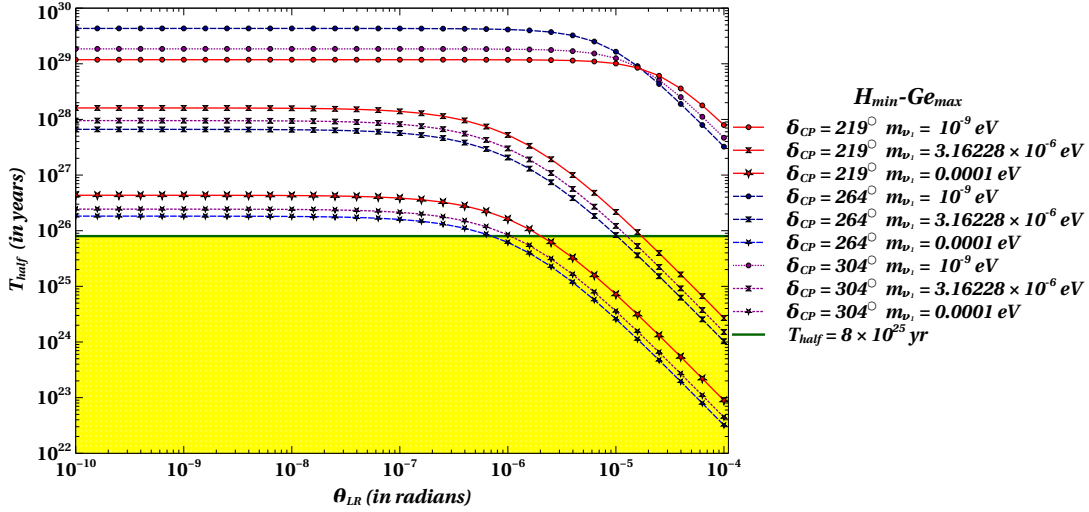


Figure 8: Half-life of $0\nu\beta\beta$ process for ^{76}Ge nucleus as a function of left-right charged gauge boson mixing for several fixed values of m_{ν_1} and δ_{CP} .

element³ is directly proportional to $e^{-i\delta_{CP}}$ and as a result one can approximately write $T_{1/2}^{0\nu} \sim \frac{1}{G_{01}^{0\nu} |M_{\nu}^{0\nu} \eta_1|^2}$. As δ_{CP} approaches 180° or 360° , the value of η_1 goes through a maxima while it becomes a minima at $\delta_{CP} = 270^\circ$. The inverse of this behaviour is reflected in the $T_{1/2}^{0\nu}$ plot. For the other lines in this figure, they receive dominant contributions from either η_λ or η_η . Here as \mathbb{U}_{13} decreases, the elements of \mathbb{S} and \mathbb{T} mixing matrices increase and hence their nature is opposite to the previous plot. The nature of the plots for ^{136}Xe nucleus is the same as the ^{76}Ge nucleus except the fact that the parameters are more tightly constrained owing to the more stringent experimental limit of the $0\nu\beta\beta$ half-life for the ^{136}Xe nucleus.

³The \mathbb{U}_{13} element will be the same as the (1,3) element of the PMNS matrix.

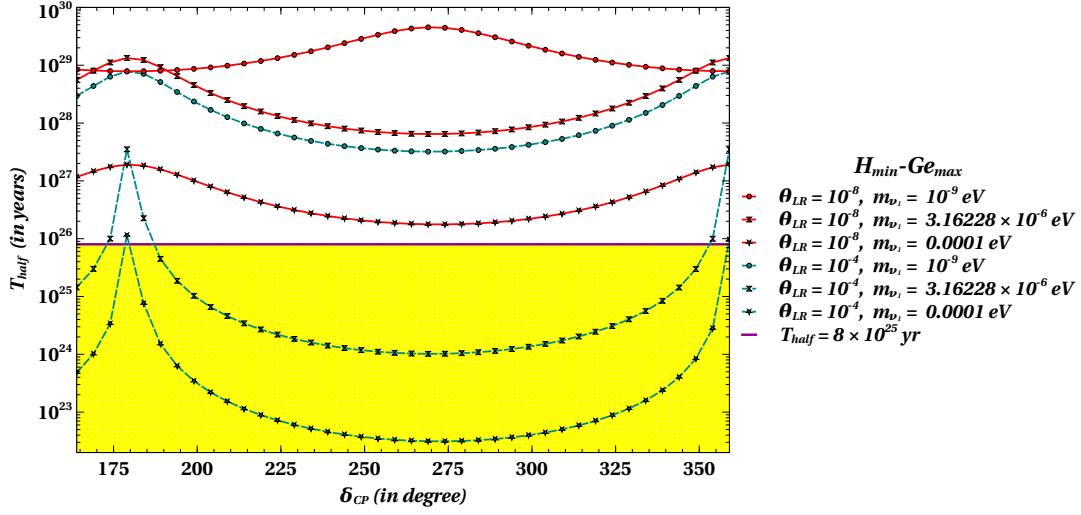


Figure 9: Half-life of $0\nu\beta\beta$ process for ^{76}Ge nucleus as a function of the CP violating phase of the PMNS matrix for several fixed values of θ_{LR} and m_{ν_1} .

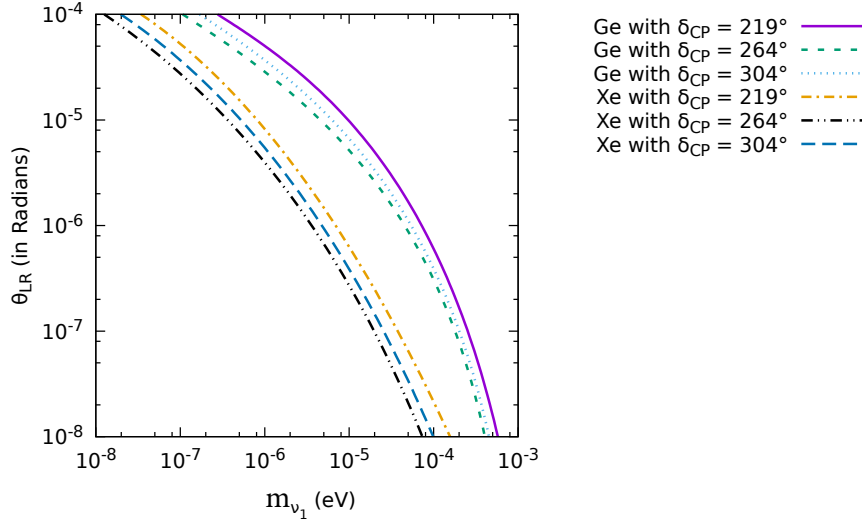


Figure 10: Limits on the lightest neutrino mass and left-right W gauge boson mixing.

Fig. 10 shows the upper limits on the mass of the lightest neutrino in this model as a function of θ_{LR} for fixed values of δ_{CP} for both ^{76}Ge and ^{136}Xe nucleus. As we have already discussed that the most stringent bound on the parameter space is obtained for a δ_{CP} of around 264° , this fact is also reflected from this figure. As expected from the previous discussion, the upper limit on the lightest neutrino mass becomes much stronger for larger values of θ_{LR} and vice-versa. This occurs due to dominant η_η contribution for a large θ_{LR} , leading to a tighter constraint on the lightest neutrino mass m_{ν_1} . Another observation is that the limits obtained for the ^{136}Xe nucleus is much stronger than the ^{76}Ge nucleus.

3 Extended Seesaw Model and Analysis

This is another extension of SM, where the model contains light and heavy sterile neutrinos⁴, which can give large contribution in $0\nu\beta\beta$ process. Several studies [42, 43, 51, 53, 69–83] have focused on sterile neutrinos with mass > 100 MeV, and large contribution in the LNV process. Here, instead we consider some of the sterile neutrino states in the < 100 MeV mass range. We investigate the allowed model parameters, which satisfy a number of theoretical and experimental constraints. In doing so, we first consider a simplistic one generation scenario with one active neutrino, one light sterile neutrino S_L , and another heavy sterile neutrino N_L . Subsequently we extend our analysis with realistic three-generation case where the neutrino sector comprises of three active neutrinos along with the additional six sterile (three S_L and three N_L) which are neutral under the SM gauge group. Below, we first review the model, and then discuss the contribution in $0\nu\beta\beta$ process.

3.1 Model

The neutral lepton sector of the model contains three generation of SM neutrinos ν_L along with additional sterile neutrino states S_L and N_L . The mass term of the neutrinos have the following form,

$$\mathcal{L} = -\frac{1}{2} \begin{pmatrix} \nu_L & S_L & N_L \end{pmatrix} \begin{pmatrix} 0 & 0 & M_D^T \\ 0 & \mu & M_S^T \\ M_D & M_S & M_R \end{pmatrix} \begin{pmatrix} \nu_L \\ S_L \\ N_L \end{pmatrix} + \text{h.c.} \quad (20)$$

We denote the neutral lepton mass matrix as \mathcal{M}_n , and hence

$$\mathcal{M}_n = \begin{pmatrix} 0 & 0 & M_D^T \\ 0 & \mu & M_S^T \\ M_D & M_S & M_R \end{pmatrix}. \quad (21)$$

We choose to work in a basis where the Majorana mass matrix M_R of N_L sterile is real. The term containing μ denotes the Majorana mass of the heavy neutrino state S_L with μ being a complex symmetric matrix. The Dirac mass matrix M_D represents the mixing between the SM neutrino states ν_L and the heavy sterile neutrino states N_L ; whereas, M_S represents the mixing between the two sterile states S_L and N_L . Throughout our analysis we consider the matrices M_R and M_S are invertible. We also assume, that, the different sub-matrices follow the hierarchy, $M_R > M_S > M_D \gg \mu$. For seesaw approximation to be valid, the mixing matrices should satisfy $\mu < M_S^T M_R^{-1} M_S$, *i.e.*, $\mu < \mathcal{O}(\frac{M_S^2}{M_R})$, see [15] for details.

Contrary to the inverse seesaw [84–95], Extended Seesaw model contains both the heavy and small lepton number violation scales M_R and μ respectively. The SM neutrino masses strongly depend on the small lepton number violating scale μ and hence in the $\mu \rightarrow 0$ limit, the ν_L states become massless. The heavy Majorana neutrino contribution in $0\nu\beta\beta$ decay can be sizeable, even in the $\mu \rightarrow 0$ limit. Hence, the contributions of the SM neutrinos and the heavy Majorana neutrinos in $0\nu\beta\beta$ process are completely decoupled from each other. Contribution from heavy sterile neutrinos for this model has been discussed in [15].

⁴We denote the gauge singlet neutrinos as sterile neutrino, as they are not charged under the SM gauge group.

The neutrino mass matrix \mathcal{M}_n can be diagonalized by a unitary transformation,

$$\mathcal{U}^T \mathcal{M}_n \mathcal{U} = \mathcal{M}_n^d, \quad (22)$$

where \mathcal{U} as an expansion with order parameter M_D/M_S has the following form [15]:

$$\begin{pmatrix} (1 - \frac{1}{2} M_D^\dagger (M_S^{-1})^\dagger M_S^{-1} M_D) W_\mu & M_D^\dagger (M_S^{-1})^\dagger W_S & M_D^\dagger M_R^{-1} W_N \\ -M_S^{-1} M_D W_\mu & (1 - \frac{1}{2} M_S^{-1} M_D M_D^\dagger (M_S^{-1})^\dagger - \frac{1}{2} M_S^\dagger M_R^{-2} M_S) W_S & M_S^\dagger M_R^{-1} W_N \\ M_S^{T-1} \mu M_S^{-1} M_D W_\mu & -M_R^{-1} M_S W_S & (1 - \frac{1}{2} M_R^{-1} M_S M_S^\dagger M_R^{-1}) W_N \end{pmatrix}. \quad (23)$$

In the above, W_μ , W_S and W_N are the three unitary matrices that diagonalize the block diagonal matrices

$$m_\nu \sim M_D^T (M_S^{-1})^T \mu (M_S)^{-1} M_D, \quad m_s \sim -M_S^T (M_R)^{-1} M_S, \quad m_n \sim M_R. \quad (24)$$

The matrix m_ν represents the light neutrino mass matrix, and m_s and m_n represent the heavy neutrino mass matrices. The hierarchy among the sub matrices ensures that m_n and its eigenvalues give the heaviest sterile neutrinos in this model. The other sterile neutrinos that originates from the diagonalization of m_s can be relatively lighter, but they certainly should be heavier than the three active neutrinos $m_\nu < m_s < m_n$. In the subsequent sections, we explore the possibility of that the sterile states from m_s are in the eV to MeV range, while the remaining sterile neutrino states m_n are more than GeV. Before presenting a detailed analysis on $0\nu\beta\beta$, we first consider additional constraints coming from light neutrino mass measurement, non-unitarity and others.

3.2 Constraints

Before delving into the analysis, we present a short descriptions of all constariants that has been applied in this model.

(a) *Theoretical Constraints:*

Hierarchy: The different sub-matrices of Eq. 20 should satisfy the hierarchy

- $M_R > M_S > M_D \gg \mu$,
- and
- $M_S^T M_R^{-1} M_S > \mu$; *i.e.*, $m_s > \mu$ (from Eq. 24), for one generation this will be $M_S^2/M_R > \mu$. This limit also defines the region where seesaw approximation is valid [15].

Unitarity: The mass matrix being symmetric, the diagonalization matrix given in Eq. 22 should be orthogonal or unitary, *i.e.*, we should have the relation $\mathcal{U}^\dagger \mathcal{U} = \mathcal{U} \mathcal{U}^\dagger = \mathbf{I}$; but working with the seesaw approximation up to a certain order and also having low scale sterile, the elements of $U = \mathcal{U} \mathcal{U}^\dagger$ will not be identity matrix rather those elements will be $\mathbf{I} \pm \delta$, where δ is the tolerance of every single elements of U to get a viable parameter space for lightest sterile⁵ in this model. So, to zero in on

⁵See analysis section.

the allowed parameter space of eV to MeV sterile in this model, we have to constrain the parameter space, setting some cut-off values on the both diagonal and non-diagonal elements of U . In short, we allow some error bar on the diagonal elements on U around unity and for non-diagonal elements the required error bar will be around zero. Depending on the choice of parameter space, the error bar may differ for diagonal and non-diagonal elements. We have generally taken the the maximum constraints on the deviation which provides us the desired allowed parameter space.

(b) *Experimental Constraint:*

Mass of active neutrino: We consider the constraint on the sum of active neutrino masses from Planck cosmological data [48], *i.e.*, at 95% C.L. the sum on the masses of active neutrinos will be less than $\sum m_\nu < 0.194$ eV. In the analysis of one-generation, this bound simply manifests as the upper bound on the mass of single active neutrino. We implement the constraints on mixing angles and on the mass square differences among three active neutrinos from neutrino oscillation data in the three-generation case [1, 96] in case of Normal hierarchy.

Constraints from $0\nu\beta\beta$ limit: The limit on the $T_{1/2}^{0\nu}$ from the KamLAND-Zen [45] severely constrains the parameter space for eV/MeV sterile of this model, see Sec. 3.3.

Daya Bay experiment: The Daya Bay reactor anti neutrino experiment shows a large exclusion region between $2 \times 10^{-4} < \Delta m_{s1}^2 < 0.3$ eV² as function of $\sin^2 2\theta_{1s}$ [97] at 95% CL, where Δm_{s1}^2 is the mass-square difference between extra sterile and electron-neutrino (ν_e) and θ_{1s} is the angle of active-sterile mixing. This result will further constrain the allowed parameter space for eV sterile.

3.3 $0\nu\beta\beta$ decay: sterile neutrino contributions

In this section, we outline the contributions of sterile neutrinos having Majorana masses in $0\nu\beta\beta$ decay.

The half-life of $0\nu\beta\beta$ is written as [15, 98]

$$\frac{1}{T_{1/2}^{0\nu}} = K_{0\nu} \left| \Theta_{ej}^2 \frac{\mu_j}{\langle p^2 \rangle - \mu_j^2} \right|^2, \quad (25)$$

where j represents the number of light neutrino states and the additional heavy neutrino states. The parameters μ_j and Θ_{ej} represent the masses of the neutrino states and the mixing with SM neutrinos respectively. In the above, $K_{0\nu} = G_{0\nu}(\mathcal{M}_N m_p)^2$ and $\langle p^2 \rangle \equiv -m_e m_p \frac{\mathcal{M}_N}{\mathcal{M}_\nu}$. The reference mass scales are considered as electron (m_e) and proton (m_p) masses, M_ν and M_N are the NMEs for exchange of light and heavy neutrinos respectively. The values of NME and phase space factor $G_{0\nu}$ have been taken from Ref. [99]. Below, we classify the sterile neutrino contributions according to its mass scale.

Other than the contributions of the SM neutrinos, the sterile neutrino states S_k and N_k ($k = 1, 2, 3$; in our case) can also contribute in the $0\nu\beta\beta$ process. Evidently, we have two extra contributions apart from the SM one.

(a) The heaviest states N_k have a mass range $m_{n_k} > 100$ -200 MeV and give a contribution in $0\nu\beta\beta$ as

$$A_N \sim \frac{V_{eN_k}^2}{m_{n_k}}, \quad (26)$$

where A_N represents the amplitude of this process, and V_{eN_k} is the mixing of the N_k states with the active neutrinos. Using $V_{eN} = M_D^\dagger M_R^{-1} W_N$, this can be simplified as

$$A_N \sim (M_D^T M_R^{-3} M_D)_{ee}. \quad (27)$$

(b) The other sterile neutrino states S_k give contributions proportional to

$$A_S \sim \frac{V_{eS_k}^2}{m_{s_k}}, \quad (28)$$

for the mass range $m_{s_k} > 100\text{-}200$ MeV, whereas

$$A_S \sim \frac{V_{eS_k}^2 m_{s_k}}{\langle p^2 \rangle}, \quad (29)$$

when sterile mass is light. We use the compact expression for the amplitude, that also take into account $\langle p^2 \rangle \simeq m_{s_k}^2 \simeq 100 \text{ MeV}^2$.

$$A_S \sim \frac{V_{eS_k}^2 m_{s_k}}{\langle p^2 \rangle - m_{s_k}^2}. \quad (30)$$

The value of m_{n_k} in our analysis is 10^5 GeV for one-generation case giving rise to active-sterile mixing as $M_D/M_R \sim 10^{-10} - 10^{-7}$, whereas m_{n_k} s are to be of the order of 50 to 500 GeV in the three-generation one having $V_{eN_k}^2$ as $\sim 10^{-8}$ to 10^{-7} . So, the sterile neutrinos N_k being heavy contributes negligibly and hence we do not consider its contribution. The half-life of $0\nu\beta\beta$ is thus,

$$\frac{1}{T_{1/2}^{0\nu}} = K_{0\nu} \left| \frac{U_{ej}^2 m_{\nu_j}}{\langle p^2 \rangle - m_{\nu_j}^2} + \frac{V_{eS_k}^2 m_{s_k}}{\langle p^2 \rangle - m_{s_k}^2} \right|^2, \quad (31)$$

where j represents the number index of three light neutrino states whereas k denotes the number index of comparatively light sterile states S_L . This is to note that, the lighter S_L states (eV-MeV) can have substantial active-sterile mixing $V_{eS} = M_D^\dagger (M_S^{-1})^\dagger W_S$.

To get the essence of all theoretical and experimental constraints properly, first we consider only one generation for all states, so the mixing matrix given in Eq. 23 will be of the order of 3×3 having M_D, M_R, M_S, μ as simply numbers.

3.4 Analysis:

3.4.1 One Generation

In this section, we provide a detailed analysis and results of the allowed range of MeV/eV sterile neutrino. In Fig. 11, the plot in the left panel (Fig. 11a) shows the allowed region for MeV sterile and its contribution to $0\nu\beta\beta$ in $M_D - M_S$ plane for one-generation scenario. The matrix \mathcal{M}_n in Eq. 21, is 3×3 instead of being 9×9 in this case. The square boxes in the index box of this figure (Fig. 11a) shows the color of allowed regions in agreement with different constraints and the respective texts are written in the same color of the border of that region. The cyan colored region enclosed by the red-dashed curve in Fig. 11a shows the region allowed by

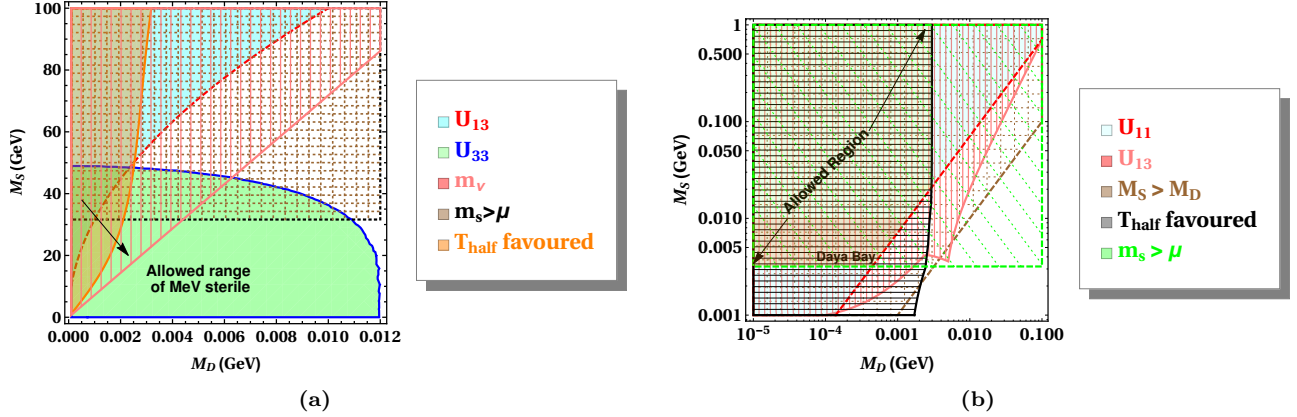


Figure 11: Allowed parameter space of light sterile neutrino in (a) MeV and in (b) eV range as function of the model parameters M_D and M_S in Extended Seesaw scheme. The regions have been obtained from theoretical constraints, light neutrino measurements and $0\nu\beta\beta$ results. The parameter μ has been set to 10^{-2} GeV and 10^{-10} GeV for MeV and eV range respectively. In both cases, $M_R = 10^5$ GeV. The orange shaded region of (b) will be constrained further from reactor anti-neutrino Daya Bay experiment [97] that will be elaborated in Fig. 12.

the off-diagonal element U_{13} , where U_{13} is the (1,3) element of $\mathcal{U}^\dagger\mathcal{U}$ with \mathcal{U} being the diagonalization matrix (Eq. 22). Here, we consider the constraint as $|U_{13}| < 10^{-8}$, *i.e.*, U_{13} is almost vanishing. The lower green region enclosed by blue solid line presents the region allowed by the diagonal element U_{33} . The constraints due to other matrix elements of U coming from the condition of diagonalization matrix \mathcal{U} being unitary are less stringent and are simply allowed by the final overlapped zone. In that final allowed region, the numerical value of off-diagonal element U_{13} is $\sim 10^{-9}$ and that of diagonal element U_{33} is $\sim (1 + 10^{-16})$. The region covered by pink-colored straight lines shows the mass of light neutrino range $0 < m_\nu < 0.194$ eV. The brown rectangle region enclosed from below by the black dashed line (near $M_S = 32$ GeV) represents the constraint $m_s = M_S^2/M_R > \mu$ marking the area where the seesaw approximation is valid. The extreme left almost vertical orange-colored region enclosed by the solid orange bow-type curve shows the region in agreement with the contribution of $0\nu\beta\beta$, where $T_{1/2}^{0\nu} > 1.07 \times 10^{26}$ yr [45]. In obtaining this allowed parameter space, we have considered both the light neutrino and sterile neutrino contribution, see Eq. 31. The values of the NMEs that we have considered in this analysis are $M_\nu = 2.29$ and $M_N = 163.5$ [99].

The overlapped region in Fig. 11a enclosed by dashed black straight line from below and solid blue line from above with $32 \text{ GeV} < M_S < 49 \text{ GeV}$ and red-dashed line from the right is the final allowed range for MeV sterile in Extended Seesaw model, with the value of $M_D \leq 0.00011$ GeV for $M_S \sim 32$ GeV and with M_D value up to ~ 0.002356 GeV for $M_S = 49$ GeV. The allowed mass range of m_s is $10 \text{ MeV} < m_s < 24$ MeV. The mass of the active neutrino in that region is $m_\nu \leq 10^{-2}$ eV.

The plot in the right panel (Fig. 11b) of Fig. 11 shows the allowed region for eV sterile in the Extended Seesaw model and its contribution to $0\nu\beta\beta$ decay in $M_D - M_S$ plane. The inclusion of sterile neutrinos whether being heavy or light has its effect on the unitarity of PMNS matrix [49]. The PMNS matrix

encoding the non-unitarity effect due to the mixings of active-sterile neutrinos is given by [49]

$$\mathcal{N} = (I - \alpha)\mathcal{U}', \quad (32)$$

where, \mathcal{U}' is equivalent to standard PMNS matrix which is also a unitary matrix having small deviation proportional α . Clearly from Eq. 23 we can see that α being theoretically same for all elements, is given by $1/2(M_D^2/M_S^2)$ in Extended Seesaw model, whereas \mathcal{U}' is equivalent to W_μ of the same equation (23). The general form of mixing terms is usually given by the ratio between the mass-scales of light neutrinos and the sterile neutrinos. Therefore, in case of light sterile (\sim eV), the active neutrino and the light sterile mass-scales being very close the effect of mixing can not be ignored. So the light sterile has strong impact on the deviation of PMNS matrix from being unitary. In the Ref. [49], the constraint on α is given for different mass values of sterile neutrinos. For the mass-square difference of sterile and active neutrinos in the eV^2 regime, at 95% CL, the bound is given by $\alpha < 10^{-2}$. So, in case of $\mathcal{N}^\dagger\mathcal{N}$ and for one-generation this bound is manifested as of the order of $\sim 10^{-4}$ as the deviation from unity (for the element U_{11}).

Therefore, in Fig. 11b, the constraint on U_{11} is taken as $|U_{11} - 1| < 10^{-4}$. Since, the matrix \mathcal{U}_{22} in Eq. 23 also contains a term like $(1 - 1/2(M_D^2/M_S^2) - 1/2(M_S^2/M_R^2))$ and M_R being heavy this term can be effectively written as $(1 - 1/2(M_D^2/M_S^2))$; so the constraint on U_{22} will be the same as that of U_{11} . The cyan-colored region surrounded by the red-dashed curve show the allowed region for an eV sterile from the limit applied on U_{11} . The pink colored region shows the allowed region for eV sterile as $|U_{13}| < 10^{-8}$. The brown-colored region shows the corresponding allowed range in agreement with the hierarchy of the model parameters $M_S > M_D$. The black-colored region depicts the allowed region from $0\nu\beta\beta$ decay [45] where contributions of eV sterile and active neutrinos have been considered. The green-colored region of oblique line shows the validity range of seesaw approximation. The final allowed region is given by the (orange + yellow) colored shaded region. The allowed region is enclosed by green line from below (at $M_S = 0.0032$ GeV, $M_D \sim 5 \times 10^{-4}$ to 0.002 GeV), by tilted red-dashed line from lower-right ($(M_D, M_S) \sim 5 \times 10^{-4}, 0.0032$ GeV up to $(M_D, M_S) \sim (0.002, 0.02)$ GeV) and finally by almost vertical black line from the right side. The region can be further extended leftwards and upwards by lowering the value of M_D and increasing the value of M_S respectively. The other constraints such as unitarity constraints from other elements of U and limit from neutrino mass is allowed by the final overlapped region. The lowest allowed value of model parameter M_S is 0.0032 GeV at $M_D = 10^{-5}$ GeV. Evidently, the lowest value of sterile neutrino from the allowed region showed in this figure is about 0.1024 eV and $m_\nu \leq 10^{-3}$ eV. In this region the $U_{11} \sim U_{22} \sim 1 + 10^{-7}$ approximately and $U_{13} \sim 10^{-9}$. The values of NMEs are the same as that of the Fig. 11a.

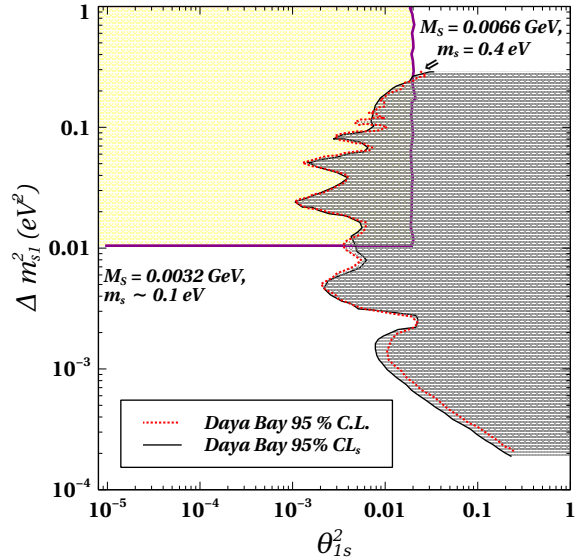


Figure 12: Constraining the region of eV sterile from Daya Bay reactor neutrino experiment. The gray-colored region from right side shows exclusion region from Daya Bay results, whereas, the yellow colored region shows the zone allowed for eV sterile.

Since, in Extended Seesaw, we have eV sterile starting from ~ 0.1 eV, the region can further be constrained from reactor anti-neutrino experiments, such as, Daya Bay. Evidently, the orange shaded region of Fig. 11b or a part of it, where we have sterile $\sim \mathcal{O}(\text{eV})$ can be probed again from such results. We represent the mentioned region of Fig. 11b of $M_S - M_D$ plane in $\Delta m_{s1}^2 (\text{eV}^2) - \theta_{1s}^2$ in the Fig. 12. The filled-in yellow box covered by the magenta color line corresponds to the aforementioned region of eV sterile of Fig. 11b. The lower line corresponds to the value $M_S = 0.0032$ GeV where as upper line corresponds to $M_S = 0.01$ GeV.

The region in Fig. 11b, below the green line and right side of the red-dashed line being completely ruled out from our model parameters (Fig. 11b) represents the white regions of Fig. 12. The dotted red and black solid line represent the Daya Bay experimental constraints on low-scale sterile in $\Delta m_{s1}^2 (\text{eV}^2) - \theta_{1s}^2$ plane [97]. The gray-colored region shows the zone that are not allowed by this experimental data. The overlapped region of this adjacent figure is ruled out from the experimental result. We can see that Daya Bay results exclude some region from the left side (giving constraint on M_D) but still allow all the values of sterile neutrino from 0.1 eV to 0.4 eV. The mass of active neutrino in the remaining allowed zone is $m_\nu \leq 10^{-4}$ eV.

In passing, we would like to comment on the active-sterile mixing value which is getting constrained from Daya Bay data. The θ_{1s}^2 is actually $(M_D/M_S)^2$. Also, from unitarity [49], we have $\frac{1}{2}(M_D/M_S)^2 < 10^{-2}$. Fig. 12 shows for some M_S, M_D values $\theta_{1s}^2 < 10^{-3}$ giving slightly more stringent bound on the mixing compared to that of coming from unitarity in our model set-up.

3.4.2 Three Generation

In Section 3.4.1, we have discussed different constraints from neutrino mass, half-life of $0\nu\beta\beta$ decay, unitarity and from the validation of seesaw approximation for one generation realisation of Extended Seesaw model. In this section, we are extending the analysis for three-generation case which is more realistic than the previous scenario. In addition to the bounds from $0\nu\beta\beta$, other experimental and theoretical constraints, we also satisfy neutrino oscillation data. In particular, we consider that,

- upper bound on the sum of all three active neutrinos is constrained from cosmology, $\sum_i m_{\nu_i} < 0.194$ eV at 2σ C.L. [48],
- two mass squared differences $6.93 < \frac{\Delta m_{21}^2}{10^{-5}} \text{eV}^2 < 7.97$ and $2.37 < \frac{\Delta m_{31}^2}{10^{-3}} \text{eV}^2 < 2.63$ vary in the 3σ range [1],
- 3σ range [1] of the three mixing angles $30^\circ < \theta_{12} < 36.51^\circ$, $37.99^\circ < \theta_{23} < 51.71^\circ$ and $7.82^\circ < \theta_{13} < 9.02^\circ$.

In the present set-up, contribution to the $0\nu\beta\beta$ can come from light active neutrinos ($m_{\nu_i}, i = 1, 2, 3$), additional eV to MeV scale sterile neutrinos ($m_{s_i}, i = 1, 2, 3$) and heavy GeV scale neutrinos ($m_{n_i}, i = 1, 2, 3$). As shown in Sec. 3.2, the contribution of heaviest sterile neutrinos to $0\nu\beta\beta$ is evidently suppressed. Here, the neutrino mass matrix is 9×9 , but we are working in the seesaw approximation regime which gives three sets of 3×3 matrices namely m_ν , m_s and m_n . After diagonalization of each 3 block of Eq. 24 individually, we check the unitarity constraints as described in Sec. 3.2 and in Sec. 3.4.1. The matrices which diagonalize each blocked-matrices combine to form a 9×9 matrix (Eq. 23) and we impose constraints on the unit

matrix (U , see Sec. 3.4.1) with the absolute variation of each elements by $\pm 10^{-2}$. This $\pm 10^{-2}$ variation manifestly impose constrains on the ratio M_D/M_S . We have checked that the error bar is consistent with the experimental bound [49] that arises due to the non-unitarity effect for eV-keV scale sterile neutrino. A detailed description of different conditions provided in Sec. 3.2 to constraint the parameter space have been thoroughly followed in the present analysis.

As discussed earlier, after using the seesaw approximation, we get three different 3×3 matrices, which are m_n, m_s, m_ν . Among them one corresponds to the mass matrix for the three active neutrinos (denoted by m_ν), other two correspond to the mass matrices for the three relatively light sterile neutrinos (denoted by m_s) and the three heavy neutrinos which are in GeV scale (denoted by m_n). From Eq. 24, we can see the expressions of m_ν, m_s and m_n depend on the matrices M_D, M_R, M_S and μ whose elements are the free input parameters in the extended seesaw scenario. We choose the model parameters in our framework in a way so that we can accommodate eV to MeV scale sterile neutrino. Before proceeding, we consider few assumptions which include M_D, M_S, M_R as the real diagonal matrices and μ as the complex symmetric matrix *i.e.* $\mu^T = \mu$ and $\mu^* \neq \mu$. In this work, we have focused on the normal hierarchy of the neutrino masses as illustrative example. In order to satisfy neutrino oscillation constraints and to obtain sterile neutrinos in eV to MeV scale, we have varied the model parameters in the following range (in GeV),

$$\begin{aligned}
10^{-5} &\leq M_{D\ ii} \leq 10^{-1}, \\
10^{-3} &\leq M_{S\ ii} \leq 10^{-1}, \\
50 &\leq M_{R\ ii} \leq 500, \\
10^{-11} &\leq \mu_{ij}^{R,I} \leq 10^{-8},
\end{aligned}
\tag{33}$$

where i, j can vary from 1 to 3. Below we show the allowed model parameters as well as correlation between different observables for this model as scatter plots.

In the left panel of Fig. 13, we have shown the allowed region in $\sum m_{\nu_i}$ (eV) – m_{s_1} (GeV) plane after satisfying all data ⁶, where m_{s_1} is the physical mass of the lightest sterile neutrino state. In the figure, green dots show the range allowed by neutrino oscillation data (N.O.D), blue rhombus points represent the range allowed by $0\nu\beta\beta$ and unitarity along with N.O.D. Finally the red points exhibit the range that is being further constrained by $m_{s_i} > \mu_i^d$. Here, m_{s_i} are the physical masses of the sterile state S_L and μ_i^d are the eigenvalues of μ and $i=1,2,3$. In the present work, the model parameters are less constrained from the $0\nu\beta\beta$ decay bound than the unitarity and $m_{s_i} > \mu_i^d$ bounds. The model parameters range considered in this work give us eV to MeV scale sterile neutrino as seen by the range of m_{s_1} -axis. One interesting thing to note here is that $m_{s_1} \geq 10^{-6}$ GeV is disallowed when we consider both the constraints, unitarity and $0\nu\beta\beta$. This is mainly due to unitarity bound since this bound mostly depends on the ratio of M_D/M_S . Therefore, when $(M_D/M_S)^2 < 10^{-2}$, those points satisfy the unitarity constraints which is $\pm 10^{-2}$ variation around the unit matrix (see Sec. 3.2). The disallowed points correspond to higher ratio, *i.e.*, $(M_D/M_S)^2 > 10^{-2}$ and those points represent lower values of the elements of μ matrix in order to satisfy the N.O.D which is not covered in Eq. 33. This also implies that the elements of M_D and M_S are of the same order for the disallowed points and more likely to have higher M_S values. Finally the red points are obtained when we impose the

⁶We get similar kind of behaviour with the other two light sterile neutrinos $s_{2,3}$. Moreover, $s_{2,3}$ also get similar kind of mass and contribute to $0\nu\beta\beta$ in equal strength.

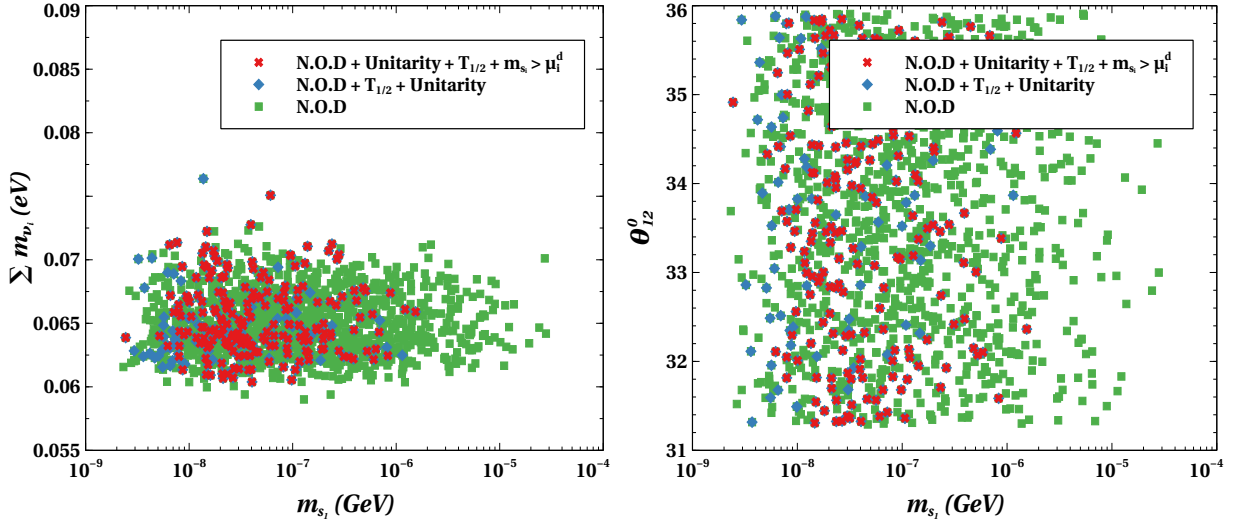


Figure 13: Scatter plots in $\sum m_{\nu_i}$ (eV) – m_{s_1} (GeV) (left panel) and θ_{12} – m_{s_1} (GeV) (right panel) planes after satisfying the constraints as mentioned in the text. N.O.D represents the constraint from neutrino oscillation data.

constraint $m_{s_i} > \mu_i^d$. After imposing this constraint, lower values of m_{s_1} are getting ruled out which are mostly in eV scale. In the right panel of this figure we have shown the variation of the solar mixing angle θ_{12} with the lightest sterile neutrino mass. We can see that the whole allowed range of θ_{12} from oscillation experiments is in agreement with all the constraints.

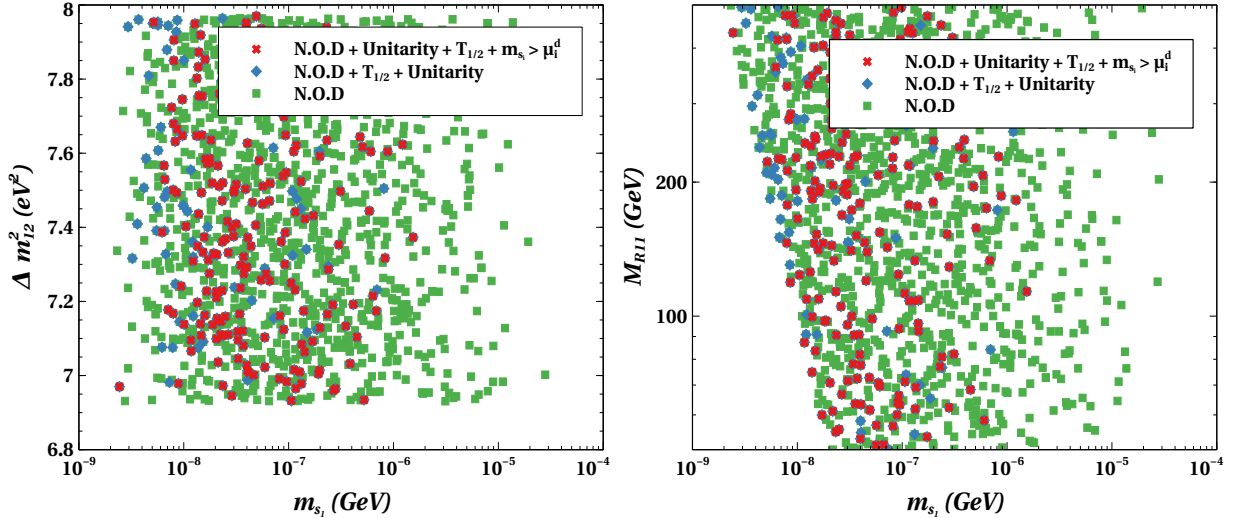


Figure 14: Scatter plots in Δm_{12}^2 (eV²) – m_{s_1} (GeV) (left panel) and M_{R11} – m_{s_1} (both are in GeV) (right panel) planes after satisfying the constraints as mentioned in the text.

In the left panel of Fig. 14, we have shown the scatter plot in Δm_{12}^2 (eV²) – m_{s_1} (GeV) plane after satisfying the constraints as mentioned in the legend of the figure. Here also the whole allowed range of Δm_{12}^2 (eV²)

from oscillation experiments satisfy all constraints. On the other hand in the right panel, we have shown the scatter plot in the $M_{R11} - m_{s1}$ plane where M_{R11} is the eigenvalue of m_n matrix because we have considered here M_R as diagonal matrix.

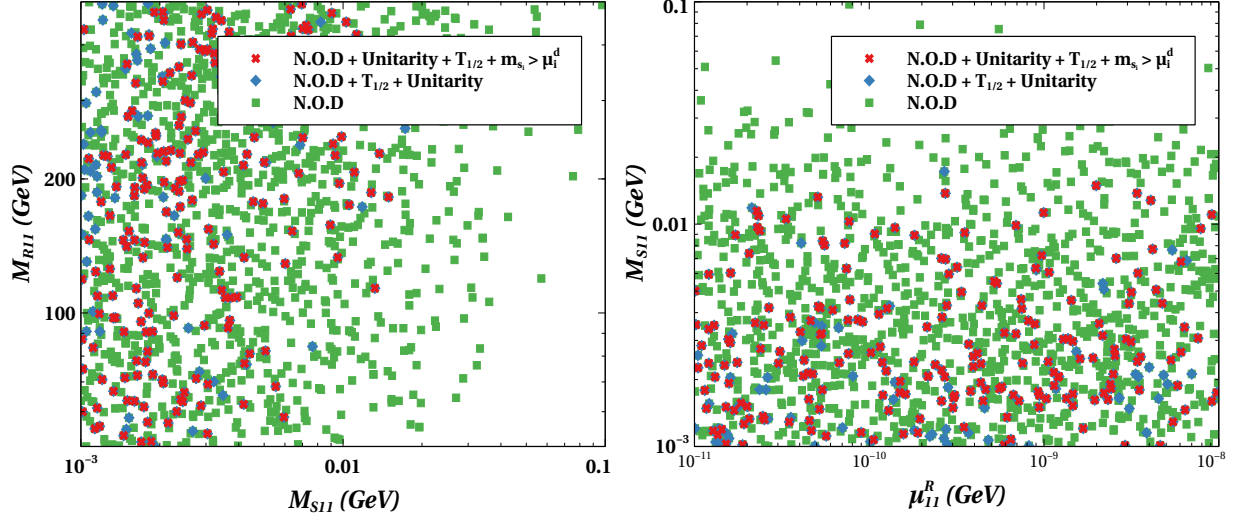


Figure 15: Scatter plots in $M_{R11} - M_{S11}$ (both in GeV) (left panel) and $M_{S11} - \mu_{11}^R$ (both in GeV) (right panel) planes after satisfying the constraints as mentioned in the text.

Left panel and right panel of Fig. 15 shows the variation in M_{R11} as function of M_{S11} and M_{S11} as function of μ_{11}^R respectively. Here, the superscript R implies real elements. In both cases $M_{S11} > 0.02$ GeV are not allowed by the unitarity constraint as mentioned earlier. The conditions coming from both unitarity and seesaw approximation can be respectively manifested as the upper and lower bound on the light sterile m_s .

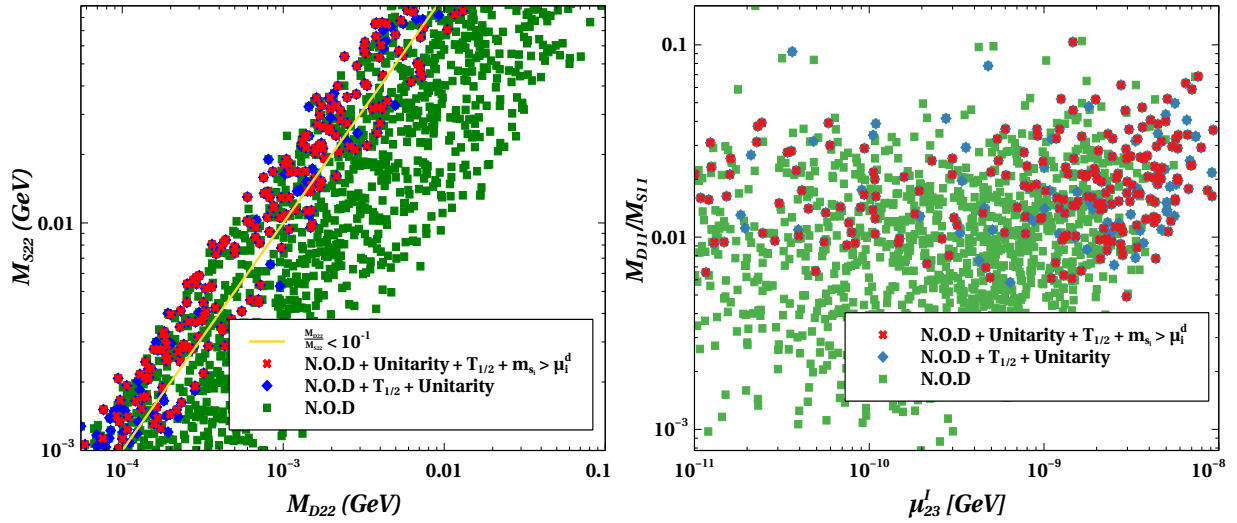


Figure 16: Scatter plots in $M_{D22} - M_{S22}$ (both in GeV) (left panel) and μ_{23}^I (GeV) $- \frac{M_{D11}}{M_{S11}}$ (right panel) planes after satisfying the constraints as mentioned in the text.

In the left and right panels of Fig. 16, we have shown the scatter plot in plane $M_{D22}-M_{S22}$ and μ_{23}^I (GeV) – $\frac{M_{D11}}{M_{S11}}$ plane respectively. Here, the superscript I denotes the imaginary part. In the left panel we can see that most of the points which satisfy oscillation data are below the yellow line which corresponds to $\frac{M_{D22}}{M_{S22}} = 10^{-1}$. As we have discussed, the unitarity bound (variation of $\pm 10^{-2}$ around unit matrix) mostly depends on the ratio $\frac{M_{Dii}}{M_{Sii}}$ ($i = 1, 2, 3$) and we can roughly say if $\frac{M_{Dii}}{M_{Sii}} < 10^{-1}$, then it can pass the unitarity bounds. One interesting thing to note here is that there exist a sharp correlation among the M_{D22} and M_{S22} parameters (which is valid for other elements of M_D and M_S matrices also). This is because, approximately $(M_D/M_S)^2 \mu \sim 10^{-11}$ GeV and we have taken $\mu < 10^{-8}$ GeV, so M_{D22} and M_{S22} can not take arbitrary values which corresponds to significant difference in their magnitudes, otherwise neutrino mass data will not be satisfied. On the other hand in the right panel of Fig. 16, we can see that after imposing all the constraints we get the points which are more prone to have higher values of μ_{23}^I . This is because when we impose the unitarity constraint which corresponds to $\frac{M_{Dii}}{M_{Sii}} < 10^{-1}$ ($i = 1, 2, 3$) and from the order of magnitude estimation of neutrino mass we obtain $\mu \gtrsim 10^{-9}$. This is clearly reflected in the right panel of the figure because the points are more dense in that region where $\mu_{23}^I \gtrsim 10^{-9}$ compared to the rest of the region.

4 Conclusion

In this work, we consider two theory frameworks with sterile neutrinos - a) Left-Right Symmetric Zee, and b) Extended Seesaw model, which successfully explain the light neutrino masses and their mixings. Both of the models can accommodate sterile neutrinos with their masses being free parameters varying over a wide range. We particularly focus on relatively lighter mass range \sim eV to MeV, and explore the contribution to $0\nu\beta\beta$ process. The Left-Right Symmetric Zee model represents a scenario where the masses of the sterile neutrinos are generated at the one loop level. They are directly dependent on the right-handed Yukawa coupling λ_R and the masses and mixings of the charged Higgs bosons. For large values of λ_R (close to the perturbative limit) the sterile neutrino masses always remain well below the MeV scale. This presents a unique scenario where the three light sterile neutrinos can have significant contribution to $0\nu\beta\beta$ process. We find that the half-life of this process crucially depends on three parameters - lightest neutrino mass m_{ν_1} , Dirac CP phase δ_{CP} , and the $W_L - W_R$ mixing angle θ_{LR} . In our analysis, we consider the cases with maximal and minimal mixings among the charged Higgs bosons and also consider both the upper and lower values of the NMEs for ^{76}Ge and ^{136}Xe nuclei. The scenario with minimal mixing of the Higgs bosons and maximum values of the NMEs produces the most stringent bound on the model. The calculated half-life for both ^{76}Ge and ^{136}Xe nuclei decreases drastically with an increase in m_{ν_1} or θ_{LR} . This is due to the dominant contributions coming from the λ and η diagrams as m_{ν_1} and/or θ_{LR} are increased. This allows us to put quite stringent bounds on both these parameters. For ^{76}Ge nucleus, the lightest neutrino mass should be less than 10^{-7} eV for $\theta_{LR} \sim 10^{-4}$ while for a lightest neutrino mass of around 10^{-3} eV the value of $\theta_{LR} \lesssim 10^{-8}$, where we consider a normal hierarchy among the active neutrino states. The bounds on ^{136}Xe nucleus are even more stringent with $m_{\nu_1} \lesssim 10^{-8}$ eV for $\theta_{LR} \sim 10^{-4}$ and $\theta_{LR} \lesssim 10^{-8}$ for $m_{\nu_1} \sim 10^{-4}$ eV. Thus we can significantly constrain the model parameters in this case from the $0\nu\beta\beta$ studies.

For the Extended seesaw, we first consider one-generation scenario where in addition to one SM neutrino two sterile neutrinos are also present. Among the two sterile neutrinos one of them is very heavy with

mass of 10^5 GeV leading to a negligible contribution in $0\nu\beta\beta$ process. The other sterile neutrino has a mass varying in between eV to MeV and this contributes significantly to the above mentioned process. We analyse a number of constraints on the model parameters, arising from $0\nu\beta\beta$, reactor anti-neutrino experiment Daya Bay, non-unitarity constraint on the mixing matrix, as well as, theory-constraints. We further extend this simplistic one-generation analysis to higher generation with three active neutrinos and six sterile neutrinos for which we satisfy the neutrino oscillation data. We present a number of correlations between the mass of the lightest sterile neutrino, model parameters and several neutrino oscillation parameters. In three-generation case, the mass of the heavy sterile states (N_s) have been varied from 50 to 500 GeV. These states give negligible contributions to $0\nu\beta\beta$ process, while the other three relatively light sterile states (S_{LS}) give substantial contributions. With the considered parameter range we obtain the upper bound on the mass of the lightest sterile neutrino S_1 as 10^{-6} GeV after imposing constraints from non-unitarity, $0\nu\beta\beta$ and others. The non-unitarity of PMNS matrix has direct impact on the mixing elements; in Extended seesaw, non-unitarity can be governed by the ratio of the bilinear mass term between active neutrino-light sterile states (M_D) to the corresponding bilinear mass terms among the sterile states (M_S). The upper bound on the ratio M_D/M_S is $\sim 10^{-1}$. We choose the effective neutrino mass scale ($\mu M_D^2/M_S^2$) to be of the order of 10^{-3} eV and we conclude in this scenario the lower bound on the elements of the complex symmetric matrix μ to be of the order of 10^{-9} GeV. Another important constraint in our scenario is $m_s > \mu$ which the seesaw approximation ceases to be valid. It evidently gives lower bound on m_{s_i} ; i.e., $\mu_{ii} > 10^{-9}$ GeV implies $m_{s_i} > 1$ eV. The masses of the other two sterile neutrinos vary as $m_{s_{2,3}} \sim \mathcal{O}(1 - 10)$ eV.

Acknowledgements: Authors acknowledge Ram Lal Awasthi for his contributions at the initial stage of this project. TJ acknowledges the support from Science and Engineering Research Board (SERB), Government of India under the grant reference no. PDF/2020/001053.

References

- [1] I. Esteban, M. C. Gonzalez-Garcia, M. Maltoni, T. Schwetz, and A. Zhou, *The fate of hints: updated global analysis of three-flavor neutrino oscillations*, *JHEP* **09** (2020) 178, [[arXiv:2007.14792](#)].
- [2] P. Minkowski, $\mu \rightarrow e\gamma$ at a Rate of One Out of 10^9 Muon Decays?, *Phys. Lett. B* **67** (1977) 421–428.
- [3] O. Sawada and A. Sugamoto, eds., *Proceedings: Workshop on the Unified Theories and the Baryon Number in the Universe: Tsukuba, Japan, February 13-14, 1979*, (Tsukuba, Japan), Natl.Lab.High Energy Phys., 1979.
- [4] S. Weinberg, *Baryon and Lepton Nonconserving Processes*, *Phys. Rev. Lett.* **43** (1979) 1566–1570.
- [5] F. Wilczek and A. Zee, *Operator Analysis of Nucleon Decay*, *Phys. Rev. Lett.* **43** (1979) 1571–1573.
- [6] S. L. Glashow, *The Future of Elementary Particle Physics*, *NATO Sci. Ser. B* **61** (1980) 687.
- [7] M. Gell-Mann, P. Ramond, and R. Slansky, *Complex Spinors and Unified Theories*, *Conf. Proc. C* **790927** (1979) 315–321, [[arXiv:1306.4669](#)].

- [8] R. N. Mohapatra and G. Senjanovic, *Neutrino Mass and Spontaneous Parity Nonconservation*, *Phys. Rev. Lett.* **44** (1980) 912.
- [9] A. Zee, *Quantum Numbers of Majorana Neutrino Masses*, *Nucl. Phys. B* **264** (1986) 99–110.
- [10] K. S. Babu, *Model of ‘Calculable’ Majorana Neutrino Masses*, *Phys. Lett. B* **203** (1988) 132–136.
- [11] E. Ma, *Pathways to naturally small neutrino masses*, *Phys. Rev. Lett.* **81** (1998) 1171–1174, [[hep-ph/9805219](#)].
- [12] F. Bonnet, M. Hirsch, T. Ota, and W. Winter, *Systematic study of the $d=5$ Weinberg operator at one-loop order*, *JHEP* **07** (2012) 153, [[arXiv:1204.5862](#)].
- [13] D. Aristizabal Sierra, A. Degee, L. Dorame, and M. Hirsch, *Systematic classification of two-loop realizations of the Weinberg operator*, *JHEP* **03** (2015) 040, [[arXiv:1411.7038](#)].
- [14] S. K. Kang and C. Kim, *Extended double seesaw model for neutrino mass spectrum and low scale leptogenesis*, *Phys. Lett. B* **646** (2007) 248–252, [[hep-ph/0607072](#)].
- [15] M. Mitra, G. Senjanovic, and F. Vissani, *Neutrinoless Double Beta Decay and Heavy Sterile Neutrinos*, *Nucl. Phys.* **B856** (2012) 26–73, [[arXiv:1108.0004](#)].
- [16] R. N. Mohapatra and J. C. Pati, *Left-Right Gauge Symmetry and an Isoconjugate Model of CP Violation*, *Phys. Rev. D* **11** (1975) 566–571.
- [17] G. Senjanovic and R. N. Mohapatra, *Exact Left-Right Symmetry and Spontaneous Violation of Parity*, *Phys. Rev. D* **12** (1975) 1502.
- [18] P. Fileviez Perez and C. Murgui, *Lepton Flavour Violation in Left-Right Theory*, *Phys. Rev. D* **95** (2017), no. 7 075010, [[arXiv:1701.06801](#)].
- [19] S. Khan, M. Mitra, and A. Patra, *Neutrino and Collider Implications of a Left-Right Extended Zee Model*, *Phys. Rev. D* **98** (2018), no. 11 115038, [[arXiv:1805.09844](#)].
- [20] A. Zee, *A Theory of Lepton Number Violation, Neutrino Majorana Mass, and Oscillation*, *Phys. Lett. B* **93** (1980) 389. [Erratum: *Phys.Lett.B* 95, 461 (1980)].
- [21] P. H. Frampton, M. C. Oh, and T. Yoshikawa, *Zee model confronts SNO data*, *Phys. Rev. D* **65** (2002) 073014, [[hep-ph/0110300](#)].
- [22] Y. Koide, *Prospect of the Zee model*, *Nucl. Phys. B Proc. Suppl.* **111** (2002) 294–296, [[hep-ph/0201250](#)].
- [23] X.-G. He, *Is the Zee model neutrino mass matrix ruled out?*, *Eur. Phys. J. C* **34** (2004) 371–376, [[hep-ph/0307172](#)].
- [24] P. Fileviez Perez, C. Murgui, and S. Ohmer, *Simple Left-Right Theory: Lepton Number Violation at the LHC*, *Phys. Rev. D* **94** (2016), no. 5 051701, [[arXiv:1607.00246](#)].
- [25] G. Karagiorgi, *Toward Solution of the MiniBooNE-LSND Anomalies*, *Nucl. Phys. B Proc. Suppl.* **229-232** (2012) 50–54.

- [26] M. Antonello et al., *Experimental search for the “LSND anomaly” with the ICARUS detector in the CNGS neutrino beam*, *Eur. Phys. J. C* **73** (2013), no. 3 2345, [[arXiv:1209.0122](#)].
- [27] **LSND** Collaboration, A. Aguilar-Arevalo et al., *Evidence for neutrino oscillations from the observation of $\bar{\nu}_e$ appearance in a $\bar{\nu}_\mu$ beam*, *Phys. Rev. D* **64** (2001) 112007, [[hep-ex/0104049](#)].
- [28] **MiniBooNE** Collaboration, A. Aguilar-Arevalo et al., *Unexplained Excess of Electron-Like Events From a 1-GeV Neutrino Beam*, *Phys. Rev. Lett.* **102** (2009) 101802, [[arXiv:0812.2243](#)].
- [29] **KARMEN** Collaboration, B. Armbruster et al., *Upper limits for neutrino oscillations muon-anti-neutrino \rightarrow electron-anti-neutrino from muon decay at rest*, *Phys. Rev. D* **65** (2002) 112001, [[hep-ex/0203021](#)].
- [30] **MINOS** Collaboration, P. Adamson et al., *Search for Sterile Neutrinos Mixing with Muon Neutrinos in MINOS*, *Phys. Rev. Lett.* **117** (2016), no. 15 151803, [[arXiv:1607.01176](#)].
- [31] **DUNE** Collaboration, B. Abi et al., *The DUNE Far Detector Interim Design Report Volume 1: Physics, Technology and Strategies*, [arXiv:1807.10334](#).
- [32] **DUNE** Collaboration, B. Abi et al., *Deep Underground Neutrino Experiment (DUNE), Far Detector Technical Design Report, Volume II: DUNE Physics*, [arXiv:2002.03005](#).
- [33] G. Mention, M. Fechner, T. Lasserre, T. Mueller, D. Lhuillier, M. Cribier, and A. Letourneau, *The Reactor Antineutrino Anomaly*, *Phys. Rev. D* **83** (2011) 073006, [[arXiv:1101.2755](#)].
- [34] K. N. Abazajian et al., *Light Sterile Neutrinos: A White Paper*, [arXiv:1204.5379](#).
- [35] F. Kaether, W. Hampel, G. Heusser, J. Kiko, and T. Kirsten, *Reanalysis of the GALLEX solar neutrino flux and source experiments*, *Phys. Lett. B* **685** (2010) 47–54, [[arXiv:1001.2731](#)].
- [36] **SAGE** Collaboration, J. Abdurashitov et al., *Measurement of the solar neutrino capture rate with gallium metal. III: Results for the 2002–2007 data-taking period*, *Phys. Rev. C* **80** (2009) 015807, [[arXiv:0901.2200](#)].
- [37] M. Drewes et al., *A White Paper on keV Sterile Neutrino Dark Matter*, *JCAP* **01** (2017) 025, [[arXiv:1602.04816](#)].
- [38] N. Sabti, J. Alvey, M. Escudero, M. Fairbairn, and D. Blas, *Refined Bounds on MeV-scale Thermal Dark Sectors from BBN and the CMB*, *JCAP* **01** (2020) 004, [[arXiv:1910.01649](#)].
- [39] E. Majorana, *Teoria simmetrica dell’elettrone e del positrone*, *Nuovo Cim.* **14** (1937) 171–184.
- [40] G. Racah, *On the symmetry of particle and antiparticle*, *Nuovo Cim.* **14** (1937) 322–328.
- [41] W. H. Furry, *On transition probabilities in double beta-disintegration*, *Phys. Rev.* **56** (1939) 1184–1193.
- [42] J. D. Vergados, H. Ejiri, and F. Šimkovic, *Neutrinoless double beta decay and neutrino mass*, *Int. J. Mod. Phys. E* **25** (2016), no. 11 1630007, [[arXiv:1612.02924](#)].
- [43] S. Dell’Oro, S. Marcocci, M. Viel, and F. Vissani, *Neutrinoless double beta decay: 2015 review*, *Adv. High Energy Phys.* **2016** (2016) 2162659, [[arXiv:1601.07512](#)].

- [44] **GERDA** Collaboration, M. Agostini et al., *Improved Limit on Neutrinoless Double- β Decay of ^{76}Ge from GERDA Phase II*, *Phys. Rev. Lett.* **120** (2018), no. 13 132503, [[arXiv:1803.11100](#)].
- [45] **KamLAND-Zen** Collaboration, A. Gando et al., *Search for Majorana Neutrinos near the Inverted Mass Hierarchy Region with KamLAND-Zen*, *Phys. Rev. Lett.* **117** (2016), no. 8 082503, [[arXiv:1605.02889](#)]. [Addendum: *Phys. Rev. Lett.* 117,no.10,109903(2016)].
- [46] **CUORE** Collaboration, C. Arnaboldi et al., *CUORE: A Cryogenic underground observatory for rare events*, *Nucl. Instrum. Meth. A* **518** (2004) 775–798, [[hep-ex/0212053](#)].
- [47] **SuperNEMO** Collaboration, R. Arnold et al., *Probing New Physics Models of Neutrinoless Double Beta Decay with SuperNEMO*, *Eur. Phys. J. C* **70** (2010) 927–943, [[arXiv:1005.1241](#)].
- [48] **Planck** Collaboration, P. A. R. Ade et al., *Planck 2015 results. XIII. Cosmological parameters*, *Astron. Astrophys.* **594** (2016) A13, [[arXiv:1502.01589](#)].
- [49] M. Blennow, P. Coloma, E. Fernandez-Martinez, J. Hernandez-Garcia, and J. Lopez-Pavon, *Non-Unitarity, sterile neutrinos, and Non-Standard neutrino Interactions*, *JHEP* **04** (2017) 153, [[arXiv:1609.08637](#)].
- [50] J. Herrero-García, T. Ohlsson, S. Riad, and J. Wirén, *Full parameter scan of the Zee model: exploring Higgs lepton flavor violation*, *JHEP* **04** (2017) 130, [[arXiv:1701.05345](#)].
- [51] J. Barry and W. Rodejohann, *Lepton number and flavour violation in TeV-scale left-right symmetric theories with large left-right mixing*, *JHEP* **09** (2013) 153, [[arXiv:1303.6324](#)].
- [52] R. L. Awasthi, M. K. Parida, and S. Patra, *Neutrino masses, dominant neutrinoless double beta decay, and observable lepton flavor violation in left-right models and $SO(10)$ grand unification with low mass W_R, Z_R bosons*, *JHEP* **08** (2013) 122, [[arXiv:1302.0672](#)].
- [53] J. Chakraborty, H. Z. Devi, S. Goswami, and S. Patra, *Neutrinoless double- β decay in TeV scale Left-Right symmetric models*, *JHEP* **08** (2012) 008, [[arXiv:1204.2527](#)].
- [54] P. S. Bhupal Dev, S. Goswami, and M. Mitra, *TeV Scale Left-Right Symmetry and Large Mixing Effects in Neutrinoless Double Beta Decay*, *Phys. Rev. D* **91** (2015), no. 11 113004, [[arXiv:1405.1399](#)].
- [55] R. N. Mohapatra, G. Senjanovic, and M. D. Tran, *Strangeness Changing Processes and the Limit on the Right-handed Gauge Boson Mass*, *Phys. Rev. D* **28** (1983) 546.
- [56] M. E. Pospelov, *FCNC in left-right symmetric theories and constraints on the right-handed scale*, *Phys. Rev. D* **56** (1997) 259–264, [[hep-ph/9611422](#)].
- [57] Y. Zhang, H. An, X. Ji, and R. N. Mohapatra, *General CP Violation in Minimal Left-Right Symmetric Model and Constraints on the Right-Handed Scale*, *Nucl. Phys. B* **802** (2008) 247–279, [[arXiv:0712.4218](#)].
- [58] A. Maiezza, M. Nemevsek, F. Nesti, and G. Senjanovic, *Left-Right Symmetry at LHC*, *Phys. Rev. D* **82** (2010) 055022, [[arXiv:1005.5160](#)].
- [59] J. Chakraborty, J. Gluza, R. Seivillano, and R. Szafron, *Left-Right Symmetry at LHC and Precise 1-Loop Low Energy Data*, *JHEP* **07** (2012) 038, [[arXiv:1204.0736](#)].

- [60] **ATLAS** Collaboration, G. Aad et al., *Search for heavy Majorana neutrinos with the ATLAS detector in pp collisions at $\sqrt{s} = 8$ TeV*, *JHEP* **07** (2015) 162, [[arXiv:1506.06020](#)].
- [61] U. Kaya, M. Sahin, and S. Sultansoy, *Majorana Neutrino and W_R at TeV scale ep Colliders*, [arXiv:1502.04115](#).
- [62] N. Arkani-Hamed, T. Han, M. Mangano, and L.-T. Wang, *Physics opportunities of a 100 TeV proton–proton collider*, *Phys. Rept.* **652** (2016) 1–49, [[arXiv:1511.06495](#)].
- [63] T. Golling et al., *Physics at a 100 TeV pp collider: beyond the Standard Model phenomena*, [arXiv:1606.00947](#).
- [64] M. Mitra, R. Ruiz, D. J. Scott, and M. Spannowsky, *Neutrino Jets from High-Mass W_R Gauge Bosons in TeV-Scale Left-Right Symmetric Models*, *Phys. Rev. D* **94** (2016), no. 9 095016, [[arXiv:1607.03504](#)].
- [65] D. Borah and A. Dasgupta, *Naturally Light Dirac Neutrino in Left-Right Symmetric Model*, *JCAP* **06** (2017) 003, [[arXiv:1702.02877](#)].
- [66] Y. Cai, T. Han, T. Li, and R. Ruiz, *Lepton Number Violation: Seesaw Models and Their Collider Tests*, *Front. in Phys.* **6** (2018) 40, [[arXiv:1711.02180](#)].
- [67] **Particle Data Group** Collaboration, J. Beringer et al., *Review of Particle Physics (RPP)*, *Phys. Rev. D* **86** (2012) 010001.
- [68] J. A. Casas and A. Ibarra, *Oscillating neutrinos and $\mu \rightarrow e, \gamma$* , *Nucl. Phys. B* **618** (2001) 171–204, [[hep-ph/0103065](#)].
- [69] W. Dekens, J. de Vries, K. Fuyuto, E. Mereghetti, and G. Zhou, *Sterile neutrinos and neutrinoless double beta decay in effective field theory*, *JHEP* **06** (2020) 097, [[arXiv:2002.07182](#)].
- [70] J. Alcaide, D. Das, and A. Santamaria, *A model of neutrino mass and dark matter with large neutrinoless double beta decay*, *JHEP* **04** (2017) 049, [[arXiv:1701.01402](#)].
- [71] O. Cremonesi, *Neutrinoless Double Beta Decay*, *J. Phys. Conf. Ser.* **718** (2016), no. 2 022006.
- [72] T. Peng, M. J. Ramsey-Musolf, and P. Winslow, *TeV lepton number violation: From neutrinoless double- β decay to the LHC*, *Phys. Rev. D* **93** (2016), no. 9 093002, [[arXiv:1508.04444](#)].
- [73] E. Lisi, A. Rotunno, and F. Simkovic, *Degeneracies of particle and nuclear physics uncertainties in neutrinoless $\beta\beta$ decay*, *Phys. Rev. D* **92** (2015), no. 9 093004, [[arXiv:1506.04058](#)].
- [74] P. S. Bhupal Dev, C.-H. Lee, and R. N. Mohapatra, *TeV Scale Lepton Number Violation and Baryogenesis*, *J. Phys. Conf. Ser.* **631** (2015), no. 1 012007, [[arXiv:1503.04970](#)].
- [75] A. Faessler, M. González, S. Kovalenko, and F. Šimkovic, *Arbitrary mass Majorana neutrinos in neutrinoless double beta decay*, *Phys. Rev. D* **90** (2014), no. 9 096010, [[arXiv:1408.6077](#)].
- [76] S. Pascoli, M. Mitra, and S. Wong, *Effect of cancellation in neutrinoless double beta decay*, *Phys. Rev. D* **90** (2014), no. 9 093005, [[arXiv:1310.6218](#)].

- [77] W.-C. Huang and J. Lopez-Pavon, *On neutrinoless double beta decay in the minimal left-right symmetric model*, *Eur. Phys. J. C* **74** (2014) 2853, [[arXiv:1310.0265](#)].
- [78] P. S. Bhupal Dev, S. Goswami, M. Mitra, and W. Rodejohann, *Constraining Neutrino Mass from Neutrinoless Double Beta Decay*, *Phys. Rev. D* **88** (2013) 091301, [[arXiv:1305.0056](#)].
- [79] S. Khan, S. Goswami, and S. Roy, *Vacuum Stability constraints on the minimal singlet TeV Seesaw Model*, *Phys. Rev. D* **89** (2014), no. 7 073021, [[arXiv:1212.3694](#)].
- [80] C. F. Wong, *Phenomenology of Sterile Neutrinos at Different Mass Scales: Neutrinoless Double Beta Decay and Neutrino Oscillations*. PhD thesis, Durham U., 2012.
- [81] J. Chakraborty, M. Das, and S. Mohanty, *Constraints on TeV scale Majorana neutrino phenomenology from the Vacuum Stability of the Higgs*, *Mod. Phys. Lett. A* **28** (2013) 1350032, [[arXiv:1207.2027](#)].
- [82] M. Mitra, G. Senjanovic, and F. Vissani, *Heavy Sterile Neutrinos and Neutrinoless Double Beta Decay*, in *47th Rencontres de Moriond on Electroweak Interactions and Unified Theories*, 5, 2012. [[arXiv:1205.3867](#)].
- [83] J. D. Vergados, H. Ejiri, and F. Simkovic, *Theory of Neutrinoless Double Beta Decay*, *Rept. Prog. Phys.* **75** (2012) 106301, [[arXiv:1205.0649](#)].
- [84] R. N. Mohapatra, *Mechanism for Understanding Small Neutrino Mass in Superstring Theories*, *Phys. Rev. Lett.* **56** (1986) 561–563.
- [85] R. N. Mohapatra and J. W. F. Valle, *Neutrino Mass and Baryon Number Nonconservation in Superstring Models*, *Phys. Rev. D* **34** (1986) 1642.
- [86] D. Wyler and L. Wolfenstein, *Massless Neutrinos in Left-Right Symmetric Models*, *Nucl. Phys. B* **218** (1983) 205–214.
- [87] E. Witten, *New Issues in Manifolds of SU(3) Holonomy*, *Nucl. Phys. B* **268** (1986) 79.
- [88] J. L. Hewett and T. G. Rizzo, *Low-Energy Phenomenology of Superstring Inspired E(6) Models*, *Phys. Rept.* **183** (1989) 193.
- [89] P. S. B. Dev and R. N. Mohapatra, *TeV Scale Inverse Seesaw in SO(10) and Leptonic Non-Unitarity Effects*, *Phys. Rev. D* **81** (2010) 013001, [[arXiv:0910.3924](#)].
- [90] S. Blanchet, P. S. B. Dev, and R. N. Mohapatra, *Leptogenesis with TeV Scale Inverse Seesaw in SO(10)*, *Phys. Rev. D* **82** (2010) 115025, [[arXiv:1010.1471](#)].
- [91] A. Ilakovac and A. Pilaftsis, *Flavor violating charged lepton decays in seesaw-type models*, *Nucl. Phys. B* **437** (1995) 491, [[hep-ph/9403398](#)].
- [92] F. Deppisch and J. W. F. Valle, *Enhanced lepton flavor violation in the supersymmetric inverse seesaw model*, *Phys. Rev. D* **72** (2005) 036001, [[hep-ph/0406040](#)].

- [93] C. Arina, F. Bazzocchi, N. Fornengo, J. C. Romao, and J. W. F. Valle, *Minimal supergravity sneutrino dark matter and inverse seesaw neutrino masses*, *Phys. Rev. Lett.* **101** (2008) 161802, [[arXiv:0806.3225](#)].
- [94] M. Malinsky, T. Ohlsson, Z.-z. Xing, and H. Zhang, *Non-unitary neutrino mixing and CP violation in the minimal inverse seesaw model*, *Phys. Lett. B* **679** (2009) 242–248, [[arXiv:0905.2889](#)].
- [95] M. Hirsch, T. Kernreiter, J. C. Romao, and A. Villanova del Moral, *Minimal Supersymmetric Inverse Seesaw: Neutrino masses, lepton flavour violation and LHC phenomenology*, *JHEP* **01** (2010) 103, [[arXiv:0910.2435](#)].
- [96] P. F. de Salas, D. V. Forero, S. Gariazzo, P. Martínez-Miravé, O. Mena, C. A. Ternes, M. Tórtola, and J. W. F. Valle, *2020 global reassessment of the neutrino oscillation picture*, *JHEP* **02** (2021) 071, [[arXiv:2006.11237](#)].
- [97] **Daya Bay** Collaboration, F. P. An et al., *Improved Search for a Light Sterile Neutrino with the Full Configuration of the Daya Bay Experiment*, *Phys. Rev. Lett.* **117** (2016), no. 15 151802, [[arXiv:1607.01174](#)].
- [98] S. Kovalenko, Z. Lu, and I. Schmidt, *Lepton Number Violating Processes Mediated by Majorana Neutrinos at Hadron Colliders*, *Phys. Rev. D* **80** (2009) 073014, [[arXiv:0907.2533](#)].
- [99] A. Meroni, S. T. Petcov, and F. Simkovic, *Multiple CP non-conserving mechanisms of $(\beta\beta)_{0\nu}$ -decay and nuclei with largely different nuclear matrix elements*, *JHEP* **02** (2013) 025, [[arXiv:1212.1331](#)].